Original Article

MOLECULAR METABOLISM

Genetic disruption of the *Gipr* in *Apoe*$^{-/-}$ mice promotes atherosclerosis

Gemma Pujadas, Laurie L. Baggio, Kiran Deep Kaur, Brent A. McLean, Xiemin Cao, Daniel J. Drucker*

ABSTRACT

Objective: The gut hormone glucose-dependent insulinotropic polypeptide (GIP) stimulates beta cell function and improves glycemia through its incretin actions. GIP also regulates endothelial function and suppresses adipose tissue inflammation through control of macrophage activity. Activation of the GIP receptor (GIPR) attenuates experimental atherosclerosis and inflammation in mice, however whether loss of GIPR signaling impacts the development of atherosclerosis is uncertain.

Methods: Atherosclerosis and related metabolic phenotypes were studied in *Apoe*$^{-/-}$:*Gipr*$^{-/-}$ mice and in *Gipr*$^{+/+}$ and *Gipr*$^{-/-}$ mice treated with an adeno-associated virus expressing PCSK9 (AAV-PCSK9). Bone marrow transplantation (BMT) studies were carried out using donor marrow from *Apoe*$^{-/-}$:*Gipr*$^{-/-}$and *Apoe*$^{-/-}$:*Gipr*$^{+/+}$mice transplanted into *Apoe*$^{-/-}$:*Gipr*$^{-/-}$ recipient mice. Experimental endpoints included the extent of aortic atherosclerosis and inflammation, body weight, glucose tolerance, and circulating lipid levels, the proportions and subsets of circulating leukocytes, and tissue gene expression profiles informing lipid and glucose metabolism, and inflammation.

Results: Body weight was lower, circulating myeloid cells were reduced, and glucose tolerance was not different, however, aortic atherosclerosis was increased in *Apoe*$^{-/-}$:*Gipr*$^{-/-}$ mice and trended higher in *Gipr*$^{-/-}$ mice with atherosclerosis induced by AAV-PCSK9. Levels of mRNA transcripts for genes contributing to inflammation were increased in the aortae of *Apoe*$^{-/-}$:*Gipr*$^{-/-}$ mice and expression of a subset of inflammation-related hepatic genes were increased in *Gipr*$^{-/-}$ mice treated with AAV-PCSK9. BMT experiments did not reveal marked atherosclerosis, failing to implicate bone marrow derived GIPR + cells in the control of atherosclerosis or aortic inflammation.

Conclusions: Loss of the *Gipr* in mice results in increased aortic atherosclerosis and enhanced inflammation in aorta and liver, despite reduced weight gain and preserved glucose homeostasis. These findings extend concepts of GIPR in the suppression of inflammation-related pathophysiology beyond its classical incretin role in the control of metabolism.

Keywords Glucose-dependant insulinotropic polypeptide receptor; Atherosclerosis; Inflammation; Incretin; Cholesterol; Blood vessel

1. INTRODUCTION

Gut hormones are secreted at low basal levels in the interprandial state, with circulating levels rising briskly in response to nutritional cues [1]. Multiple gut hormones contribute signals regulating food intake, pancreatic enzyme secretion and digestion, gastrointestinal motility, nutrient absorption, and disposal. Two of the most extensively studied gut hormones, glucose-dependent insulinotropic polypeptide (GIP) and glucagon-like peptide-1 (GLP-1) exhibit incretin-like activity, and potentiate meal-stimulated insulin release to facilitate glucose uptake and control of peripheral glucose production [2]. GLP-1 also exerts a number of complementary actions to improve metabolism, including inhibition of glucagon secretion, reduction of gastric emptying, and promotion of satiety, enabling weight loss [3]. These actions of GLP-1 have supported the development of degradation-resistant GLP-1R agonists (GLP-1RA) for the treatment of people with type 2 diabetes (T2D) and obesity [4].

Both GIP and GLP-1 act through structurally related yet distinct G protein coupled receptors expressed in islet β-cells, as well as in extrapancreatic tissues [2,5]. Among the most extensively studied effects of GLP-1 are its actions in the cardiovascular system. Preclinical studies demonstrated that GLP-1 receptor (GLP-1R) activation reduces the severity of experimental stroke, atherosclerosis, and myocardial infarction [6–8], actions thought to reflect the activity of the GLP-1R in the heart, blood vessels, and the immune system [9,10]. Importantly, cardiovascular outcome trials examining the safety of multiple GLP-1RA demonstrate a reduction in the rates of major adverse cardiovascular events (MACE) in people with T2D [11]. These findings support the safety of GLP-1RA in people at high risk of developing, or with pre-existing cardiovascular disease.

The corresponding development of GIP-based therapeutics has been more challenging, due in part to the more restricted actions of GIP, and observations that the insulinotropic activity of GIP is diminished in people with T2D [12]. Furthermore, substantial preclinical data, using

Lunenfeld-Tanenbaum Research Institute, Mt. Sinai Hospital, University of Toronto, Ontario Canada M5G1X5

*Corresponding author. LTRI, Mt. Sinai Hospital 600 University Ave Mailbox 39, TCP5-1004 Toronto ON M5G 1X5 Canada. E-mail: drucker@lunenfeld.ca (D.J. Drucker).

Abbreviations: MACE, major adverse cardiovascular events; GIPR, Glucose-dependent insulinotropic polypeptide receptor; AAV-PCSK9, Adeno-associated virus proprotein convertase subtilisin/kexin type 9; GFP, Green fluorescent protein; NEFAs, non-esterified fatty acids; BMT, bone marrow transplantation; GTT, glucose tolerance test; ORO, oil red O

Received June 25, 2022 • Revision received August 17, 2022 • Accepted August 26, 2022 • Available online 31 August 2022

https://doi.org/10.1016/j.molmet.2022.101586

GIP receptor (GIPR) antagonists, or mouse genetics to inactivate the genes for GIP or the GIPR, reveals that loss of GIP activity is also associated with resistance to weight gain, and improved insulin sensitivity [13–15]. Hence, there remains some uncertainty as to whether GIPR agonism, or antagonism, represents the most promising strategy for therapy of metabolic disorders such as T2D or obesity.

The GIPR is also expressed in the heart, blood vessels, and the immune system [16–20], and loss of GIPR activity enhances adipose tissue inflammation via upregulation of alarmin expression within macrophages [19]. However, much less is known about the cardiovascular actions of GIP. Activation of the GIPR has little effect in mice with experimental coronary artery occlusion, whereas reduction of GIPR expression in cardiomyocytes was associated with cardioprotection in mice with acute myocardial infarction [16]. GIPR agonism also reduces vascular inflammation and decreases the development of atherosclerosis in mice prone to develop accelerated atherosclerosis [21–23]. However, much less is known about the potential vascular consequences of reduced GIPR signalling. Here we studied the development of atherosclerosis and inflammation in several different models of *Gipr*$^{-/-}$ mice with accelerated atherosclerosis.

2. MATERIALS AND METHODS

2.1. Mice and diets

All mouse studies were performed in accordance with protocols approved by the Sinai Health System and The Centre for Phenogenomics (TCP; Toronto, ON, Canada; AUP# 24–0045H). All experiments were carried out in groups of male mice on a C57BL/6J genetic background. Wild-type littermates or wild-type mice from the same colony were used as controls.

Mice were maintained on a 12 h light/dark cycle at an ambient temperature of 21 °C, with free access to food and water, except where noted. Mice were fed either a standard rodent chow diet (RCD; 18% kcal from fat, 2018 Harlan Teklad, Mississauga, ON) or a proatherogenic diet (42% high fat diet (HFD), 0.2% total cholesterol, TD. 88137, Envigo).

The generation and characterization of *Gipr*$^{-/-}$ mice was described previously [24]. *Apoe*$^{-/-}$ mice were purchased from Jackson Laboratories (Stock #2052). *Apoe*$^{-/-}$:*Gipr*$^{-/-}$ double knockout mice were generated by crossing *Gipr*$^{-/-}$ mice with *Apoe*$^{-/-}$ mice and subsequent mating of heterozygote progeny. An established PCSK9-AAV protocol for generating hypercholesterolemia and atherosclerosis [25] was used in *Gipr*$^{-/-}$ and wild type *Gipr*$^{+/+}$ littermate *AAV.mPcsk9* mice. pAAV/D377-mPCSK9 (plasmid # 58376; donated by Jacob Bentzon, Aarhus University, Aarhus, Denmark [26]) was obtained from Addgene and produced with an AAV8 vector (AAV8.ApoEHCR-hAAT.D377Y-mPCSK9.bGH, Penn Vector Core in the Gene Therapy Program of the University of Pennsylvania). As a control, *Gipr*$^{-/-}$+ *AAV.GFP* mice were generated using pAAV.CMV.PI.EGFP.WPRE.bGH (plasmid # 105530, Addgene) incorporated into an AAV8 vector (AAV8.TBG.PI.eGFP.WPRE.bGH, Penn Vector Core in the Gene Therapy Program of the University of Pennsylvania). All mice received a single tail vein injection of 3×10^{11} viral genome copies.

2.2. Body composition using MRI (magnetic resonance imaging)

Body composition (total fat and lean mass) was measured prior to and every 4 weeks after placing mice on the proatherogenic HFD, using a mouse whole-body Echo MRI nuclear magnetic resonance system (Echo Medical Systems, Houston, TX).

2.3. Blood and tissue analyses

For terminal studies, mice were sacrificed by CO_2 inhalation, blood was obtained by cardiac puncture and tissues were dissected and immediately frozen in liquid nitrogen. Liver samples for histology were fixed in 10% neutral buffered formalin for 48 h, transferred to 70% ethanol, paraffin-embedded, sectioned at 4 μm and stained with hematoxylin and eosin using standard protocols. Whole aortae were collected at the time of sacrifice and fixed overnight in 10% neutral buffered formalin. Atherosclerotic lesions were detected by staining with Sudan IV (MilliporeSigma, S-8756) and imaged as described [27]. Aortic roots were isolated and processed for histology as described [28]. Serial sections in which all 3 aortic valves were clearly visible were stained for Oil Red O, Masson's Trichrome, Von Kossa, F4/80, and Moma-2 using standard protocols. ImageJ software was used to quantify staining.

All blood samples (50–100 μl) for measuring insulin, non-esterified fatty acids (NEFAs), cholesterol, and triglycerides (TGs) at the indicated time points during metabolic tests were collected from the tail vein into lithium coated Microvette tubes (Sarstedt, Numbrecht, Germany) and mixed with a 10% volume of TED (5000 kIU/mL Trasylol, 32 mM EDTA, and 0.1 mM Diprotin A). Blood samples for plasma cytokine measurements were collected by cardiac puncture at the time of sacrifice and mixed with a 10% volume of TED. For complete blood counts, ~200 μl of peripheral blood was collected from the tail vein into EDTA coated Microvette tubes (Sarstedt, Numbrecht, Germany) and kept at room temperature until processed for cell isolation. Isolation and quantification of peripheral blood mononuclear cells was carried out using methods and antibodies described in our laboratory [24].

2.4. Glucose and lipid tolerance tests

For oral glucose tolerance tests (oGTT), mice were fasted for 5 h (9am-2pm) and then D-Glucose (2 g/kg; Sigma, Oakville, ON) was administered by oral gavage. Blood glucose was measured in tail vein samples using a handheld glucose meter (Contour, Bayer, Mississauga, ON) at baseline (time 0) and 15, 30, 45, 60, 90 and 120 min post-glucose administration. For oral lipid tolerance tests (oLTT), mice were fasted overnight (5pm-9am) and then animals received a 200 μl oral gavage of olive oil (Sigma) and blood samples were collected from the tail vein prior to (time 0) and 1, 2, and 3 h after olive oil gavage. Plasma was collected from blood samples via centrifugation (>12,000 rpm, 4 °C, 5 min) and stored at −80 °C until analysed.

2.5. Fasting and refeeding studies

Mice were fasted overnight (5pm-9am) with free access to water. The following morning, a fasting blood sample (100 μl) was collected from the tail vein and mice were given free access to food for 1 h, after which a second blood sample (100 μl) was collected from the tail vein.

2.6. Metabolic and cytokine assays

Plasma insulin levels were measured using an Ultrasensitive Mouse Insulin ELISA kit (Cat# 80-INSMSU-E01 Alpco Diagnostics, Salem, NH). Plasma NEFAs were assayed using the NEFA-HR (2) kit (FUJIFILM Wako Pure Chemical Corp., Cat# 999–34691, 995–34791, 991–34891, 993–35191, 276–76491). Plasma TGs were determined by enzymatic assay using the TRIGL B kit and calibrator (Roche Diagnostics, Cat# 05171407, 10759350). Plasma cholesterol levels were assayed using a Wako Cholesterol E kit (FUJIFILM Wako Diagnostics U.S.A. Corporation, Cat# 999–02601). Plasma cytokines were quantified using a V-Plex Proinflammatory Panel 1 Mouse Kit (Mesoscale, Cat# K15048D).

For assessment of TG and cholesterol levels in tissue, frozen liver samples were weighed (10–20 mg) and lipids were extracted using a 2:1 chloroform-methanol solution, dried under N_2 and reconstituted in 50 µl of 3:2 tert-butyl alcohol:triton X-100/methyl alcohol (1:1). Hepatic TG and cholesterol levels were quantified using the TRIGL B assay kit and Wako Cholesterol E kit, respectively, and normalized to tissue weight.

2.7. Bone marrow transplantation (BMT)

Bone marrow chimeras were generated by irradiating 8-week-old *Apoe*$^{-/-}$:*Gipr*$^{-/-}$ recipient males (1,100 cGy, split into two equal doses separated 4h apart) followed by tail vein injection of 5×10^6 congenic bone marrow cells from *Apoe*$^{-/-}$ or *Apoe*$^{-/-}$:*Gipr*$^{-/-}$ donor males, as described [29].

2.8. RNA isolation and gene expression analysis

For RNA extraction, tissue samples were homogenized in TRI Reagent (Molecular Research Center, Cincinnati, ON) using a TissueLyser II system (Qiagen, Germantown, MD). cDNA synthesis and Real-time quantitative PCR (RT-qPCR) were carried out as previously described [30]. A list of qPCR primers and associated ID numbers is provided in Supplementary Table 1. RT-qPCR data was analysed using the $2^{-\Delta\Delta Ct}$ method, and levels of mRNA transcripts were normalized to *Ppia* (peptidylprolyl isomerase A-cyclophilin A).

2.9. Statistical analysis

Data are presented as the mean ± SD or as the mean ± SEM, as indicated. Statistical comparisons were made by one- or two-way ordinary ANOVA followed by Bonferroni post hoc or by unpaired two-tailed Student's t-test using GraphPad Prism version 8 Software (San Diego, CA). A P value ≤ 0.05 was considered statistically significant.

3. RESULTS

To probe the consequences of extinguishing GIP action for the development of experimental atherosclerosis, we mated *Gipr*$^{-/-}$ mice with *Apoe*$^{-/-}$ mice to generate *Apoe*$^{-/-}$:*Gipr*$^{-/-}$ mice. The extent of aortic atherosclerosis was studied in *Gipr*$^{+/+}$, *Gipr*$^{-/-}$, *Apoe*$^{-/-}$ and *Apoe*$^{-/-}$:*Gipr*$^{-/-}$ mice after 19 weeks of HFD feeding (Supplementary Fig. 1A). Consistent with previous findings of resistance to weight gain in *Gipr*$^{-/-}$ mice [24,31], both *Gipr*$^{-/-}$ and *Apoe*$^{-/-}$:*Gipr*$^{-/-}$ mice exhibited reduced body weight gain, and decreased liver and white adipose tissue mass (Supplementary Figs. 1B-L and 2A). Despite reduced body weight in *Gipr*$^{-/-}$ and *Apoe*$^{-/-}$:*Gipr*$^{-/-}$ mice, there were no genotype-dependent differences in levels of plasma glucose, non-esterified fatty acids (NEFAs), triglycerides, or cholesterol (Supplementary Figs. 2B–E). Although glucose and lipid tolerance and plasma levels of NEFAs were not consistently different across genotypes, glucose-stimulated insulin levels were lower during the oGTT, and lower in the fasted and fed state, consistent with reduced body weight in *Apoe*$^{-/-}$:*Gipr*$^{-/-}$ mice (Supplementary Figs. 2F–K).

Despite reduced body weight and comparable metabolic profiles, the burden of aortic plaque was increased in *Apoe*$^{-/-}$:*Gipr*$^{-/-}$ mice (Figure 1A) and the extent of aortic macrophage infiltration (F4/80) and collagen content (quantified by Masson's Trichrome staining) trended higher (Figure 1B). We next analysed the aortic expression of genes important for inflammation, cholesterol metabolism and endothelial function. Notably, expression of *S100a8*, but not *S100a9*, alarmins suppressed by GIP in adipose tissue macrophages [19], was very low, but increased in the aortae of *Apoe*$^{-/-}$:*Gipr*$^{-/-}$ mice (Figure 1C). Furthermore, mRNA transcripts for *Adgr1e*, *Mgl2*, *Ccr2*, and *Tnf*, were upregulated in the aortae of *Apoe*$^{-/-}$:*Gipr*$^{-/-}$ mice (Figure 1C). *Pecam1*, *Nos3,* and *Acta2b* mRNA transcripts related to endothelial function were not different in the aortae of *Apoe*$^{-/-}$:*Gipr*$^{-/-}$ vs. *Apoe*$^{-/-}$ mice (Figure 1D). Levels of aortic mRNA transcripts for *Abca1* and *Abcg1*, encoding proteins regulating lipid transport, were not different, whereas mRNA levels of *Hmgcs2*, a gene important for carbohydrate and lipid metabolism, were reduced in the aortae from *Apoe*$^{-/-}$:*Gipr*$^{-/-}$ mice (Figure 1E). Additionally, there were no significant differences in mRNA expression levels of immune cell-type-specific markers in *Apoe*$^{-/-}$:*Gipr*$^{-/-}$ vs. *Apoe*$^{-/-}$ mice, although levels of *Itgam*, a marker of myeloid cells, were upregulated in *Apoe*$^{-/-}$ and *Apoe*$^{-/-}$:*Gipr*$^{-/-}$ mice (Supplementary Fig. 3A).

As GIPR signalling regulates hematopoiesis and myelopoiesis [30,32], which in turn may contribute to the development of atherosclerosis [33], we next examined circulating immune cells. The proportion of B cells and T cells was reduced, whereas circulating myeloid cells, and CD11b + cells, a marker for macrophages, granulocytes, and NK cells, were increased in both *Apoe*$^{-/-}$ and *Apoe*$^{-/-}$:*Gipr*$^{-/-}$ mice (Figure 2A,B). However, the percentage of myeloid and Cd11b + cells was significantly lower in *Apoe*$^{-/-}$:*Gipr*$^{-/-}$ vs. *Apoe*$^{-/-}$ mice (Figure 2A,B). Consistent with previous findings [30], circulating levels of Ly6C- cells (that delineate patrolling myeloid cells) were increased in *Gipr*$^{-/-}$ mice (Figure 2D), however no other genotype-dependent differences were detected in circulating levels of neutrophils, monocytes, or any of the other blood cell subsets (Figure 2C,D). Moreover, we saw no significant differences in circulating levels of inflammatory cytokines in *Apoe*$^{-/-}$:*Gipr*$^{-/-}$ vs. *Apoe*$^{-/-}$ mice, suggesting that loss of GIPR signalling does not affect systemic inflammation in our experimental model (Supplementary Fig. 3A).

GIP modulates lipolysis and lipogenesis within adipose tissue, actions with indirect implications for lipid flux in organs such as liver [34,35]. Although the livers from *Apoe*$^{-/-}$:*Gipr*$^{-/-}$ mice appeared visibly healthier (Figure 2E), hepatic triglycerides were not different, whereas hepatic cholesterol content was increased in *Apoe*$^{-/-}$:*Gipr*$^{-/-}$ mice (Figure 2F,G). Hepatic mRNA transcripts for *Abca1* were increased in *Apoe*$^{-/-}$:*Gipr*$^{-/-}$ mice, however levels of several mRNA transcripts encoding proteins important for cholesterol metabolism were not differentially expressed in livers from *Apoe*$^{-/-}$ vs. *Apoe*$^{-/-}$:*Gipr*$^{-/-}$ mice (Figure 2H). Interestingly, levels of hepatic mRNA transcripts for proteins contributing to control of glucose and lipid metabolism, such as *Pck1*, *Pgc1a*, *Foxo1*, *Hnf4a*, *Mlxipl*, and *Ppara* were increased and *Pparg* was reduced in *Apoe*$^{-/-}$:*Gipr*$^{-/-}$ mice (Figure 2I). However, as noted, fasting glycemia and glucose tolerance were not different in *Apoe*$^{-/-}$:*Gipr*$^{-/-}$ mice (Supplementary Figs. 2B and G). No consistent genotype-dependent differences were observed in hepatic mRNA levels of genes that regulate inflammation (Figure 2J).

To interrogate the phenotype arising from loss of *Gipr* in a second independent experimental model of atherosclerosis, we treated groups of *Gipr*$^{+/+}$ and *Gipr*$^{-/-}$ mice with an adeno-associated virus expressing proprotein convertase subtilisin/kexin type 9 (AAV-PCSK9). Mice were maintained on a pro-atherogenic diet to induce dyslipidemia and atherosclerosis for 23 weeks (Supplementary Fig. 4A) [26]. Once again, the extent of body weight gain and adiposity was attenuated, and liver and WAT weights were reduced in AAV-PCSK9-treated *Gipr*$^{-/-}$ vs *Gipr*$^{+/+}$ mice (Supplementary Figs. 4B–D, G–N). Plasma cholesterol and triglyceride levels were progressively increased in AAV-PCSK9-treated vs. AAV-GFP-treated mice (Supplementary Figs. 4E and F). For these analyses, we considered the data to be meaningfully different when values obtained for AAV-PCSK9-treated *Gipr*$^{-/-}$ mice were significantly different from AAV-

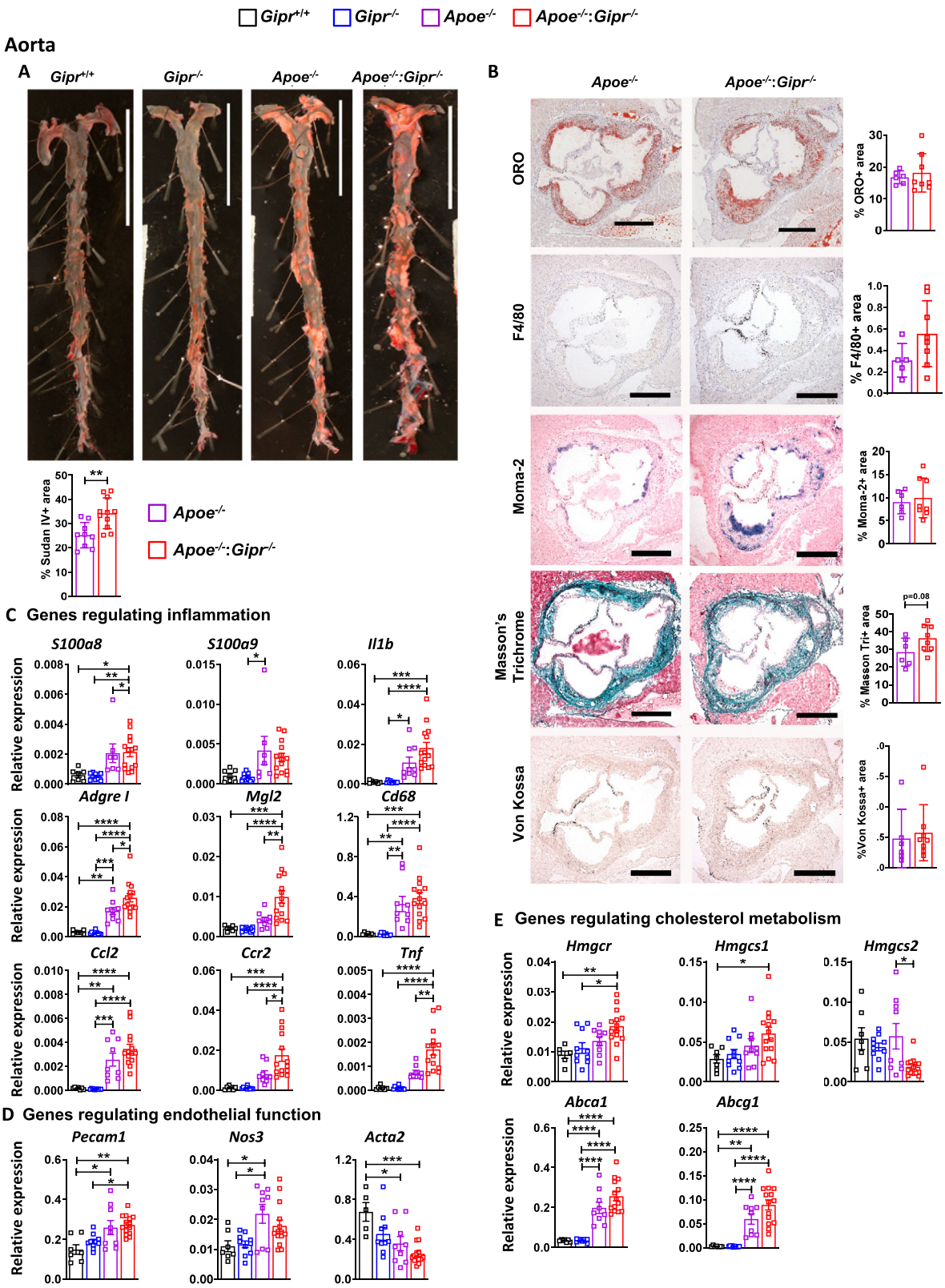

Figure 1: Aortic plaque area and inflammation are greater in *Apoe*$^{-/-}$:*Gipr*$^{-/-}$ compared to control mice. *Gipr*$^{+/+}$(*Wild type*), *Gipr*$^{-/-}$, *Apoe*$^{-/-}$ and *Apoe*$^{-/-}$:*Gipr*$^{-/-}$ mice were fed a proatherogenic diet for 19 weeks. Representative images and quantification of **(A)** whole mount en face aortae stained with Sudan IV for detection of atherosclerotic plaques, and **(B)** aortic root sections stained for Oil Red O (ORO), F4/80, Moma-2, Masson's Trichrome, and Von Kossa (magnification, X5). Aortic mRNA expression levels of genes related to **(C)** inflammation, **(D)** endothelial function, and **(E)** cholesterol metabolism. Data are mean ± SD (panels A and B) or ± SEM (panels C–E). n = 5–14 mice per group. * $P \leq 0.05$, ** $P \leq 0.01$, *** $P \leq 0.001$, **** $P \leq 0.0001$. No atherosclerosis or related structural abnormalities was detected in the aortae of wild-type or *Gipr*$^{-/-}$ mice.

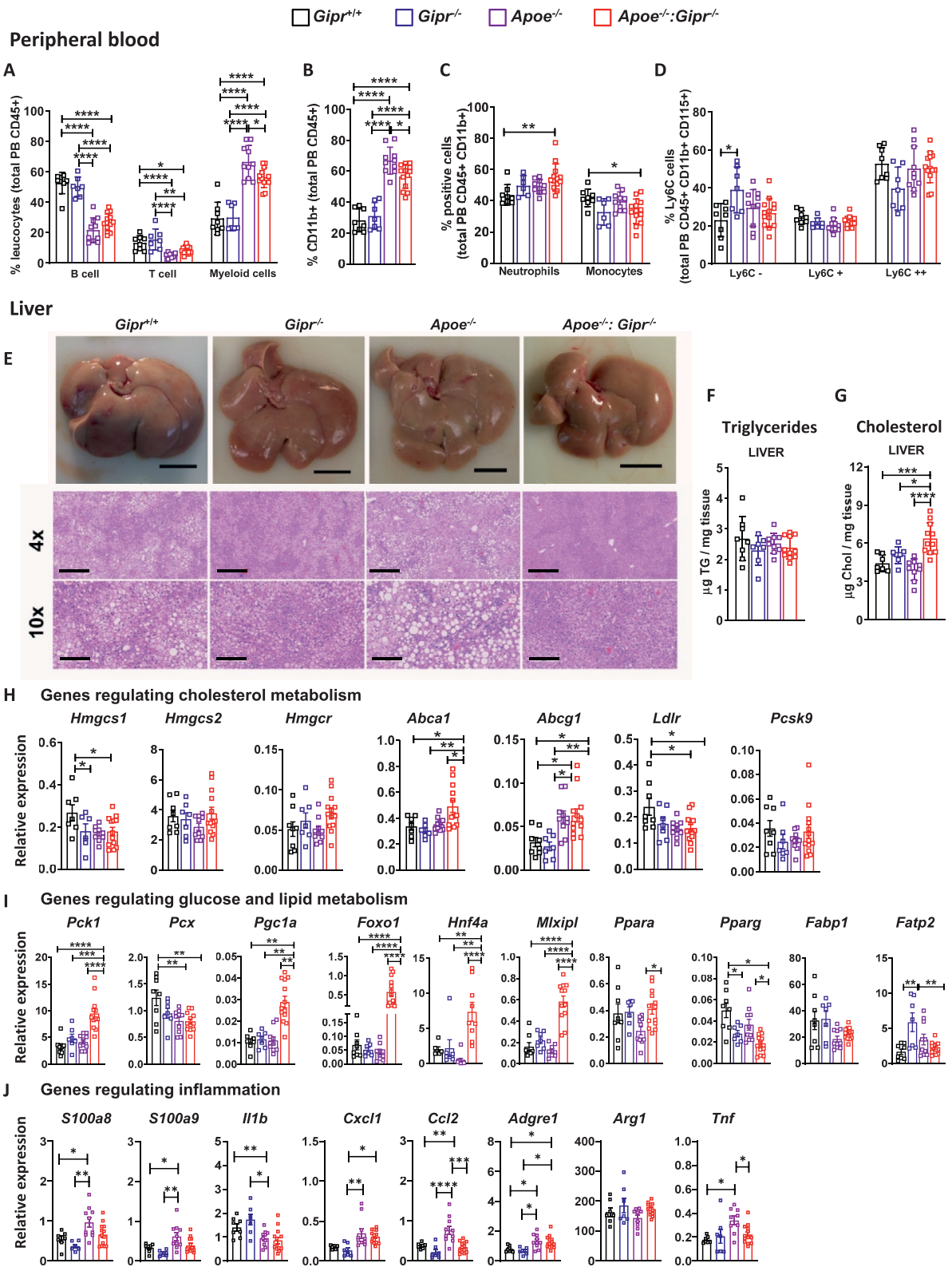

Figure 2: Peripheral blood immune cell populations and hepatic lipid and gene expression profiles in *Gipr*$^{+/+}$, *Gipr*$^{-/-}$, *Apoe*$^{-/-}$ and *Apoe*$^{-/-}$:*Gipr*$^{-/-}$ mice following 19 weeks of proatherogenic diet feeding. (A–D) Proportions of circulating immune cells. **(E)** Representative whole liver (top panel) and H&E-stained liver sections (bottom panels). Hepatic triglyceride **(F)** and cholesterol **(G)** levels. Hepatic mRNA expression levels of genes related to **(H)** cholesterol metabolism, **(I)** glucose and lipid metabolism, and **(J)** inflammation. Data are mean ± SD (panels A–D, F and G) or ± SEM (panels H–J). n = 7–13 mice per group. * $P \leq 0.05$, ** $P \leq 0.01$, *** $P \leq 0.001$, **** $P \leq 0.0001$.

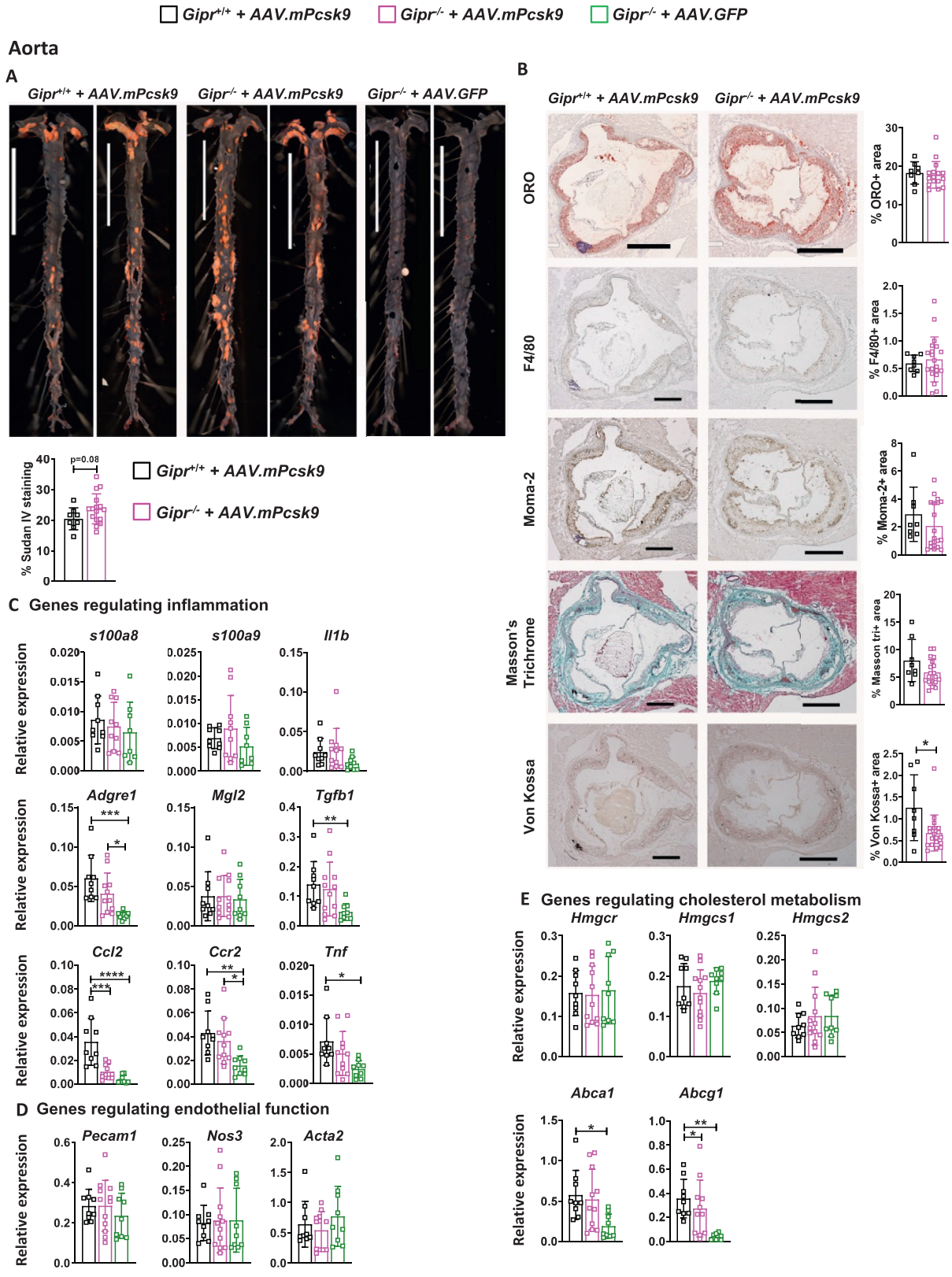

Figure 3: Atherosclerosis is not exacerbated in PCSK9-treated *Gipr*$^{-/-}$ mice. *Gipr*$^{+/+}$ (*Wild type*) and *Gipr*$^{-/-}$ mice were treated with PCSK9 (AAV.mPcsk9) or control (AAV.GFP) adeno-associated virus and then maintained on a proatherogenic diet for 23 weeks. Representative images and quantification of **(A)** whole mount en face aortae stained with Sudan IV for detection of atherosclerotic plaques, and **(B)** aortic root sections stained for Oil Red O (ORO), F4/80, Moma-2, Masson's Trichrome, and Von Kossa (magnification, X5). Aortic mRNA expression levels of genes related to **(C)** inflammation, **(D)** endothelial function, and **(E)** cholesterol metabolism. Figure 3 A Sclae bar = 1 cm; Figure 3B, scale bars = 500 μm. Data are mean ± SD. n = 8–20 mice per group. * $P \leq 0.05$, ** $P \leq 0.01$, *** $P \leq 0.001$, **** $P \leq 0.0001$.

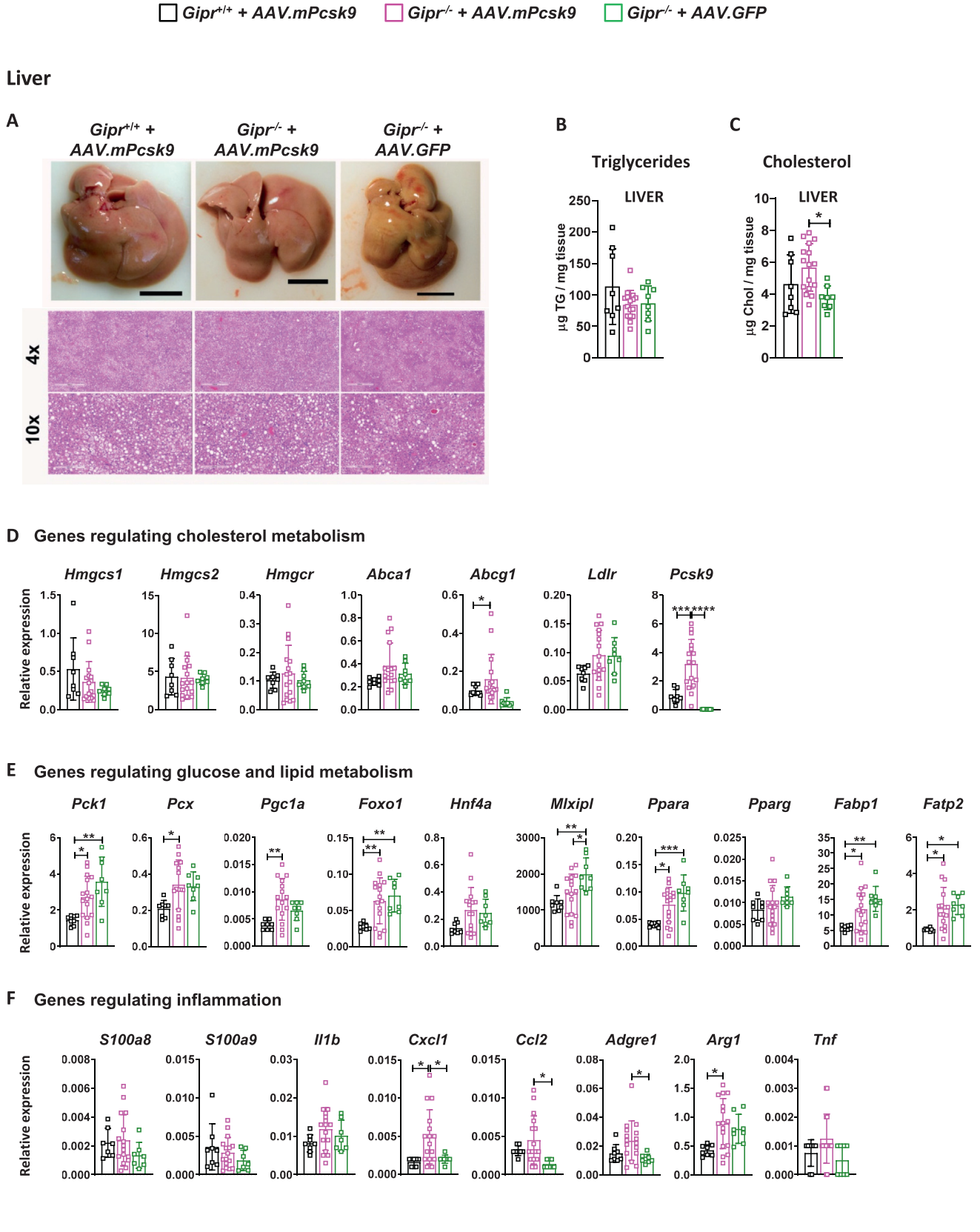

Figure 4: Analysis of liver tissue from PCSK9-treated *Gipr*$^{-/-}$ and control mice maintained on a proatherogenic diet. (A) Representative whole liver (top panel) and H&E-stained liver sections (bottom panels) from *Gipr*$^{+/+}$ and *Gipr*$^{-/-}$ mice that were treated with PCSK9 (AAV.mPcsk9) or control (AAV.GFP) adeno-associated virus and fed a proatherogenic diet for 23 weeks. Hepatic triglyceride **(B)** and cholesterol **(C)** levels. Hepatic mRNA expression levels of genes related to **(D)** cholesterol metabolism, **(E)** glucose and lipid metabolism, and **(F)** inflammation. For (A) tp panel, scale bar - 1cm, bottom 2 histology panels scale bars = 500 µm. Data are mean ± SD. n = 8–16 mice per group. * $P \leq 0.05$, ** $P \leq 0.01$, *** $P \leq 0.001$, **** $P \leq 0.0001$.

PCSK9-treated *Gipr*$^{+/+}$ and AAV-GFP-treated *Gipr*$^{-/-}$ mice. Metabolically, plasma glucose, NEFAs, triglycerides, cholesterol, and oral glucose and lipid tolerance were not different in AAV-PCSK9-treated *Gipr*$^{-/-}$ mice (Supplementary Fig. 5). Aortic plaque area was greater following administration of AAV-PCSK9 (Figure 3A, top panel), and trended higher but was not different in AAV-PCSK9-treated *Gipr*$^{-/-}$ vs. *Gipr*$^{+/+}$ mice (Figure 3A, bottom panel). Although the extent of aortic calcification (Von Kossa staining) was reduced in AAV-PCSK9-treated *Gipr*$^{-/-}$ vs. *Gipr*$^{+/+}$ mice, no differences in aortic levels of lipid, macrophage or collagen staining were observed (Figure 3B). The majority of inflammation-related genes were not differentially expressed in the aortae from AAV-PCSK9-treated *Gipr*$^{-/-}$ vs. *Gipr*$^{+/+}$ mice (Figure 3C). Similarly, although levels of *Abcg1* mRNA transcripts were reduced in aortae from AAV-PCSK9-treated *Gipr*$^{-/-}$ mice, most mRNA transcripts examined encoding proteins involved in cholesterol metabolism or endothelial function were not differentially expressed in aortae from AAV-PCSK9-treated *Gipr*$^{-/-}$ vs. *Gipr*$^{+/+}$ mice (Figure 3D, E). Likewise, there were no significant differences in mRNA levels of immune cell-type-specific markers or plasma cytokine levels in AAV-PCSK9-treated *Gipr*$^{-/-}$ mice (Supplementary Fig. 3B).

The gross and histological appearance of the livers from AAV-PCSK9-treated *Gipr*$^{-/-}$ vs. *Gipr*$^{+/+}$ mice were not different and hepatic triglycerides were similar; however, cholesterol levels were higher in AAV-PCSK9-treated *Gipr*$^{-/-}$ mice (Figure 4A–C). Levels of hepatic mRNA transcripts for genes controlling cholesterol metabolism were not different in AAV-PCSK9 vs. AAV-GFP-treated *Gipr*$^{-/-}$ mice (Figure 4D). Although several genotype-dependent differences were observed in hepatic mRNA levels of genes that regulate glucose and lipid metabolism, there were no significant differences between AAV-PCSK9-treated *Gipr*$^{-/-}$ mice and both AAV-PCSK9-treated *Gipr*$^{+/+}$ and AAV-GFP-treated *Gipr*$^{-/-}$ mice (Figure 4E). Analysis of genes encoding biomarkers of inflammation revealed increased levels of mRNA transcripts for *Cxcl1* and *Arg1* in AAV-PCSK9-treated *Gipr*$^{-/-}$ mice; however, mRNA levels of *S100a8*, *S100a9*, *Il1b*, *Ccl2*, *Adgre1*, and *Tnf* were not different in livers from AAV-PCSK9-treated *Gipr*$^{-/-}$ vs. *Gipr*$^{+/+}$ mice (Figure 4F).

Previous studies revealed a role for bone marrow-derived GIPR + cells in control of inflammation, in part through suppression of macrophage activation [19,30]. To determine whether loss of the *Gipr* contributes to increased aortic inflammation and atherosclerosis in *Apoe*$^{-/-}$:*Gipr*$^{-/-}$ mice through bone marrow-dependent mechanisms, we transplanted bone marrow from *Apoe*$^{-/-}$:*Gipr*$^{-/-}$and *Apoe*$^{-/-}$:*Gipr*$^{+/+}$mice into *Apoe*$^{-/-}$:*Gipr*$^{-/-}$ recipient mice (Supplementary Fig. 6A). Circulating B cells were reduced and T cells were increased; however, myeloid cells, including neutrophils, monocytes, CD11b + cells, and proportions of Ly6C+, Ly6C- and Ly6C++ cell subpopulations were not different in *Apoe*$^{-/-}$:*Gipr*$^{-/-}$ mice transplanted with *Gipr*$^{+/+}$ (*Apoe*$^{-/-}$:*Gipr*$^{-/-\text{Gipr}+/+\text{BM}}$) vs. *Gipr*$^{-/-}$ (*Apoe*$^{-/-}$:*Gipr*$^{-/-\text{Gipr}-/-\text{BM}}$) bone marrow (Supplementary Fig. 6B). Similarly, body weight gain, body composition, glucose tolerance, glucose-stimulated insulin levels, and plasma NEFAs, triglycerides, and cholesterol were not different in *Apoe*$^{-/-}$:*Gipr*$^{-/-\text{Gipr}+/+\text{BM}}$ vs. *Apoe*$^{-/-}$:*Gipr*$^{-/-\text{Gipr}-/-\text{BM}}$ mice (Figure 5A–C).

Surprisingly, the extent of aortic plaque was modest, and not different in *Apoe*$^{-/-}$:*Gipr*$^{-/-\text{Gipr}+/+\text{BM}}$ vs. *Apoe*$^{-/-}$:*Gipr*$^{-/-\text{Gipr}-/-\text{BM}}$ mice (Figure 5D). In contrast to evidence for increased aortic inflammation detected in *Apoe*$^{-/-}$:*Gipr*$^{-/-}$ mice (Figure 1), no differences were observed in multiple mRNA biomarkers of inflammation assessed in aortae from *Apoe*$^{-/-}$:*Gipr*$^{-/-\text{Gipr}+/+\text{BM}}$ vs. *Apoe*$^{-/-}$:*Gipr*$^{-/-\text{Gipr}-/-\text{BM}}$ mice (Supplementary Fig. 6C). Similarly, no consistent differences were detected in the expression profiles for hepatic genes contributing to control of inflammation or glucose and lipid metabolism in *Apoe*$^{-/-}$:*Gipr*$^{-/-\text{Gipr}+/+\text{BM}}$ vs. *Apoe*$^{-/-}$:*Gipr*$^{-/-\text{Gipr}-/-\text{BM}}$ mice (Supplementary Fig. 7).

4. DISCUSSION

Studies of GIP action in animals demonstrated that hyperglycemia was associated with downregulation of GIP receptor expression in pancreatic islets and defective GIP action [36,37], while attenuation of the insulinotropic action of GIP was also observed in people with T2D [12]. Nevertheless, partial restoration of GIP action was demonstrated in individuals with T2D following treatment with insulin for several weeks to improve glucose control [38], renewing interest in the possibility of GIPR agonism for the therapy of T2D. Paradoxically however, pharmacological blockade of the GIPR has also been associated with favourable metabolic phenotypes in small animals and non-human primates [15], engendering simultaneous interest in the development of GIPR antagonists alone, or in combination with GLP-1 receptor agonists [39], for the treatment of obesity or T2D [13]. Given the importance of understanding the cardiovascular safety of new therapeutic agents under development for diabetes or obesity, our current studies were originated to examine the consequences of inactivation of the *Gipr* on the development of experimental atherosclerosis in mice. Interestingly, we detected increased aortic atherosclerosis together with upregulated expression of genes encoding pro-inflammatory proteins within the aorta of *Apoe*$^{-/-}$:*Gipr*$^{-/-}$ mice, despite concomitant resistance to diet-induced weight gain and lower insulin levels in *Apoe*$^{-/-}$:*Gipr*$^{-/-}$ vs. *Apoe*$^{-/-}$ mice. Moreover, circulating levels of cholesterol and triglycerides, and lipid tolerance were not different in *Apoe*$^{-/-}$:*Gipr*$^{-/-}$ vs. *Apoe*$^{-/-}$ mice. The increased burden of aortic atherosclerosis and inflammation detected in the setting of reduced body weight raised the possibility that loss of the previously described suppressive actions of GIP on bone marrow-derived macrophage activity [19,30] contributed to the development of atherosclerosis and aortic inflammation in *Apoe*$^{-/-}$:*Gipr*$^{-/-}$ mice.

The inability to detect substantial atherosclerosis or differences in the extent of aortic atherosclerosis in *Apoe*$^{-/-}$:Gipr$^{-/-\text{Gipr}+/+\text{BM}}$ mice vs. *Apoe*$^{-/-}$:*Gipr*$^{-/-\text{Gipr}-/-\text{BM}}$ mice likely reflects the actions of radiation to attenuate the development of murine atherosclerosis. Several studies have demonstrated that bone marrow transplantation attenuates weight gain and results in reduced aortic lesion burden in *Ldlr*$^{-/-}$ and *Apoe*$^{-/-}$ mice [40,41], as well as decreased aortic inflammation [42]. Mechanistically, these observations in atherosclerosis-prone mice have been linked to reduction of LDL uptake within the intima, reducing the extent of lipid accretion, foam cell accumulation, lesion formation, and subsequent local inflammation within the aortic arch [43]. Hence our hypothesis, based on earlier studies [19,30], that loss of the myeloid GIPR contributes to macrophage activation and acceleration of aortic inflammation and atherosclerosis cannot be substantiated from the current data and will require additional studies, such as genetic targeting of *Gipr* within macrophages in mice with atherosclerosis, to pursue these possibilities without the complications of BMT.

An unexpected finding accompanying enhanced atherosclerosis was the increased expression of pro-inflammatory genes in the aorta of *Apoe*$^{-/-}$:*Gipr*$^{-/-}$ mice, including higher levels of mRNA transcripts for the macrophage marker *Adgre1* (encoding F4/80) and the alarmin *S100a8*, as well as cytokines and chemokines central to the inflammatory process. These observations resemble findings made in independent studies demonstrating a role for loss of the GIPR in promoting macrophage activation, via activation of S100a8 and S100a9, within adipose tissue, observations attributed to bone

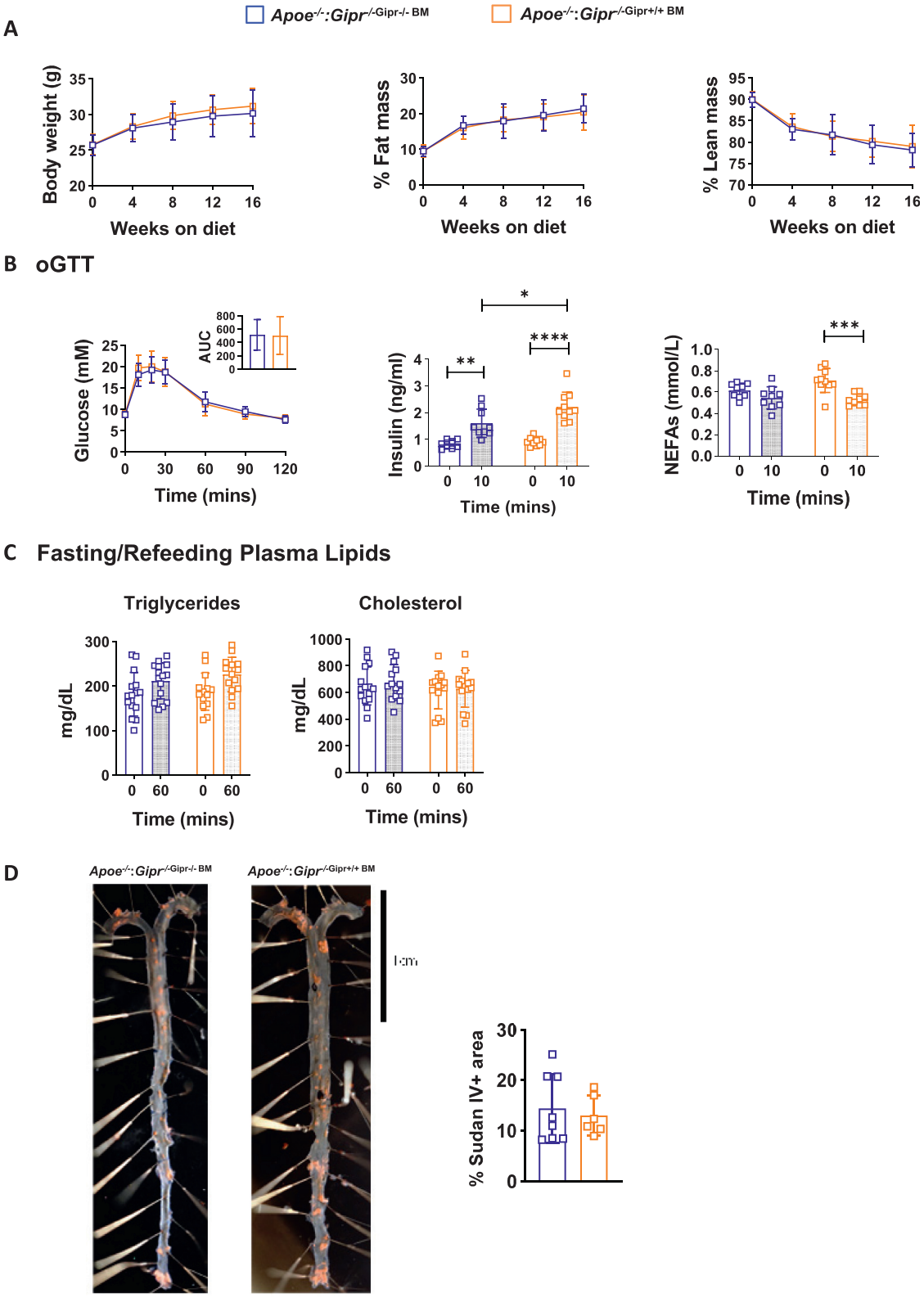

Figure 5: Restoration of *Gipr* expression in the bone marrow compartment does not modify atherosclerosis severity in *Apoe*$^{-/-}$:*Gipr*$^{-/-}$ mice. *Apoe*$^{-/-}$:*Gipr*$^{-/-}$ mice received a bone marrow transplant from *Apoe*$^{-/-}$:*Gipr*$^{-/-}$ (*Apoe*$^{-/-}$:*Gipr*$^{-/-\text{Gipr}-/-\text{BM}}$) or *Apoe*$^{-/-}$:*Gipr*$^{+/+}$ (*Apoe*$^{-/-}$:*Gipr*$^{-/-\text{Gipr}+/+\text{BM}}$) mice and then maintained on a proatherogenic diet for 19 weeks. **(A)** body weight and body composition measured every 4 weeks. **(B)** Blood glucose levels during an oral glucose tolerance test (oGTT; left panel), plasma insulin (middle panel) and non-esterified fatty acid (NEFAs, right panel) levels prior to (time 0) and at 10 min post-glucose administration. **(C)** Plasma triglyceride and cholesterol levels following an overnight fast (time 0) and after 1 h (time 60 min) of refeeding. **(D)** Representative images and quantification of whole mount en face aortae stained with Sudan IV for detection of atherosclerotic plaques. Data are mean ± SD. n = 6–14 mice per group. * $P \leq 0.05$, ** $P \leq 0.01$, *** $P \leq 0.001$, **** $P \leq 0.0001$.

marrow-derived myeloid precursors through the use of BMT experiments [19,30]. Although we were unable to conclude, due to the results of the BMT studies, that a related process contributes to enhanced macrophage activity in the aorta of GIPR-deficient mice, this possibility remains reasonable and merits further investigation, perhaps using atherosclerosis-prone mice with selective GIPR deficiency in myeloid cells.

The available preclinical data supports a beneficial role for GIPR agonism in reducing the extent of atherosclerosis, and vascular inflammation in mice [21,22], whereas deletion of the *Gipr* exaggerated the extent of vascular injury in mice following femoral artery wire injury [44]. Some, but not all [45] studies have correlated the levels of circulating GIP or variants in the GIPR with the risk of developing cardiovascular disease, including atherosclerosis and stroke [46]. Short term infusion of GIP in humans increased the expression of proinflammatory cytokines and chemokines in subcutaneous adipose tissue and in the circulation [47]. Two rare missense GIPR variants, R190Q (rs139215588) and E288G (rs143430880) associate with increased systolic blood pressure, reduced BMI, yet no consistent change in risk of cardiovascular events [48]. In contrast, analysis of genetic variation at the GIP and GIPR genes using Mendelian Randomization revealed an association between predicted augmentation of GIP-GIPR signaling and reduced levels of cardiometabolic risk factors such as C reactive protein, triglycerides, and increased levels of HDL cholesterol, beyond that predicted from a reduced risk of T2D [49].

The interest in understanding the putative link between directional changes in GIPR signaling and the risk of cardiovascular disease has been heightened by the clinical approval of tirzepatide, a potent GIPR-GLP-1R co-agonist with substantial efficacy in people with T2D and/or obesity [50]. Tirzepatide produces substantial reduction of HbA1c and weight loss, associated with reduction in blood pressure, circulating lipids and some biomarkers associated with cardiometabolic risk [51]. A pre-specified meta-analysis of cardiovascular events in the SURPASS trials assessing the efficacy of tirzepatide in people with T2D revealed a reduction in major adverse cardiovascular events in tirzepatide-treated subjects, although the number of events was insufficient to draw definitive conclusions [52]. The cardiovascular safety of tirzepatide is being compared to dulaglutide in the SURPASS-CVOT trial (NCT04255433) in people with T2D, expected to complete in October 2024.

5. LIMITATIONS AND FUTURE DIRECTIONS

Our studies have several limitations. First, we used mice with germline disruption of the *Gipr* gene, and it is possible that developmental compensation arising in these mice impacted one or more metabolic phenotypes under study. Our studies did not include mice with experimental diabetes, which might modify the importance of loss of the *Gipr* for control of metabolism and atherosclerosis. The mice analyzed following bone marrow transplantation exhibited very little aortic atherosclerosis, diminishing the potential utility of these experiments for inferring the role of bone marrow-derived cells in the pathophysiology of aortic inflammation and atherosclerosis in $Gipr^{-/-}$ mice. Moreover, $Apoe^{-/-}$ mice exhibit dysregulated lipid metabolism from birth, whereas induction of dyslipidemia using AAV-PCSK9 occurs later in life starting at 8 weeks of age, precluding a direct comparison of results from these distinct models. Furthermore, it is possible that the trend of increased atherosclerosis in AAV-PCSK9-treated $Gipr^{-/-}$ mice may have become significant if a larger experimental cohort was analyzed. Finally, we did not interrogate the impact of GIPR antagonists on the development of atherosclerosis, experiments that may have more translational relevance for clinical development of GIPR antagonists or unimolecular combinations of GIPR antagonists and GLP-1R agonists for the treatment of diabetes and obesity [13]. In summary, our current data linking loss of GIPR signaling to enhanced atherosclerosis and vascular inflammation, taken together with published studies reporting reduced atherosclerosis with GIPR agonists [21,53], extends our understanding of mechanisms linking directional changes in GIPR activity to control of atherosclerosis.

AUTHOR CONTRIBUTIONS

Conceptualization, G.P. and D.J.D.; Investigation, G.P., L.L.B., X.C., B. M., and K.K.; Formal Analysis and Visualization, G.P.; D.J.D. — Original Draft, D.J.D. — Review & Editing, G.P., L.L.B., K.K., and D.J.D.; Funding Acquisition and Project Administration, D.J.D.; Supervision, D.J.D. D.J.D. takes primary responsibility for the data described in this manuscript.

CONFLICT OF INTEREST

DJD has served as a consultant or speaker within the past 12 months to Altimmune, Amgen, Applied Molecular Transport, Eli Lilly Inc., Kallyope, Merck Research Laboratories, Novo Nordisk Inc., and Pfizer Inc. None of the other authors has competing interests. Investigator-initiated research for studies of GLP-1 and GIP are supported in part by grants from Novo Nordisk Inc and Pfizer to Mt. Sinai Hospital and DJD.

DATA AVAILABILITY

Data will be made available on request.

ACKNOWLEDGEMENTS

D.J.D. was supported by a CIHR Foundation Grant 154321, an investigator-initiated operating grant from Novo Nordisk Inc, the Novo Nordisk Foundation-Sinai Health Fund in Incretin biology, the Canada—Israel Health Research Initiative, jointly funded by the Canadian Institutes of Health Research, the Israel Science Foundation, the International Development Research Centre, and the Azrieli Foundation, and the Banting and Best Diabetes Centre-Novo Nordisk Chair in Incretin biology. We thank KW Annie Bang, Mt. Sinai Hospital, for expert assistance with flow cytometry analyses.

APPENDIX A. SUPPLEMENTARY DATA

Supplementary data to this article can be found online at https://doi.org/10.1016/j.molmet.2022.101586.

REFERENCES

[1] Drucker, D.J., 2016. Evolving concepts and translational relevance of enteroendocrine cell biology. The Journal of Cinical Endocrinology and Metabolism 101(3):778—786.

[2] Campbell, J.E., Drucker, D.J., 2013. Pharmacology physiology and mechanisms of incretin hormone action. Cell Metabolism 17(4):819—837.

[3] Sandoval, D.A., D'Alessio, D.A., 2015. Physiology of proglucagon peptides: role of glucagon and GLP-1 in health and disease. Physiological Reviews 95(2): 513—548.

[4] Drucker, D.J., Habener, J.F., Holst, J.J., 2017. Discovery, characterization, and clinical development of the glucagon-like peptides. Journal of Clinical Investigation 127(12):4217—4227.

[5] Baggio, L.L., Drucker, D.J., 2007. Biology of incretins: GLP-1 and GIP. Gastroenterology 132(6):2131—2157.

[6] During, M.J., Cao, L., Zuzga, D.S., Francis, J.S., Fitzsimons, H.L., Jiao, X., et al., 2003. Glucagon-like peptide-1 receptor is involved in learning and neuroprotection. Nature Medicine 9(9):1173—1179.

[7] Rakipovski, G., Rolin, B., Nohr, J., Klewe, I., Frederiksen, K.S., Augustin, R., et al., 2018. The GLP-1 analogs liraglutide and semaglutide reduce atherosclerosis in ApoE(-/-) and LDLr(-/-) mice by a mechanism that includes inflammatory pathways. JACC Basic Transl Sci 3(6):844—857.

[8] Noyan-Ashraf, M.H., Momen, M.A., Ban, K., Sadi, A.M., Zhou, Y.Q., Riazi, A.M., et al., 2009. GLP-1R agonist liraglutide activates cytoprotective pathways and improves outcomes after experimental myocardial infarction in mice. Diabetes 58(4):975—983.

[9] Ussher, J.R., Drucker, D.J., 2012. Cardiovascular biology of the incretin system. Endocrine Reviews 33(2):187—215.

[10] Drucker, D.J., 2016. The cardiovascular biology of glucagon-like peptide-1. Cell Metabolism 24(1):15—30.

[11] Sattar, N., Lee, M.M.Y., Kristensen, S.L., Branch, K.R.H., Del Prato, S., Khurmi, N.S., et al., 2021. Cardiovascular, mortality, and kidney outcomes with GLP-1 receptor agonists in patients with type 2 diabetes: a systematic review and meta-analysis of randomised trials. Lancet Diabetes & Endocrinology 9(10):653—662.

[12] Nauck, M.A., Heimesaat, M.M., Orskov, C., Holst, J.J., Ebert, R., Creutzfeldt, W., 1993. Preserved incretin activity of glucagon-like peptide 1 [7-36 amide] but not of synthetic human gastric inhibitory polypeptide in patients with type-2 diabetes mellitus. Journal of Clinical Investigation, 91301—91307.

[13] Killion, E.A., Lu, S.C., Fort, M., Yamada, Y., Veniant, M.M., Lloyd, D.J., 2020. Glucose-dependent insulinotropic polypeptide receptor therapies for the treatment of obesity, do agonists = antagonists? Endocrine Reviews 41(1).

[14] Killion, E.A., Chen, M., Falsey, J.R., Sivits, G., Hager, T., Atangan, L., et al., 2020. Chronic glucose-dependent insulinotropic polypeptide receptor (GIPR) agonism desensitizes adipocyte GIPR activity mimicking functional GIPR antagonism. Nature Communications 11(1):4981.

[15] Killion, E.A., Wang, J., Yie, J., Shi, S.D., Bates, D., Min, X., et al., 2018. Anti-obesity effects of GIPR antagonists alone and in combination with GLP-1R agonists in preclinical models. Science Translational Medicine 10(472).

[16] Ussher, J.R., Campbell, J.E., Mulvihill, E.E., Baggio, L.L., Bates, H.E., McLean, B.A., et al., 2018. Inactivation of the glucose-dependent insulinotropic polypeptide receptor improves outcomes following experimental myocardial infarction. Cell Metabolism 27(2):450—460.

[17] Baggio, L.L., Yusta, B., Mulvihill, E.E., Cao, X., Streutker, C.J., Butany, J., et al., 2018. GLP-1 receptor expression within the human heart. Endocrinology 159(4):1570—1584.

[18] Pujadas, G., Drucker, D.J., 2016. Vascular biology of glucagon receptor superfamily peptides: mechanistic and clinical relevance. Endocrine Reviews 37(6):554—583.

[19] Mantelmacher, F.D., Zvibel, I., Cohen, K., Epshtein, A., Pasmanik-Chor, M., Vogl, T., et al., 2019. GIP regulates inflammation and body weight by restraining myeloid-cell-derived S100A8/A9. Nature Metabolism 1(1):58—69.

[20] Varol, C., Zvibel, I., Spektor, L., Mantelmacher, F.D., Vugman, M., Thurm, T., et al., 2014. Long-acting glucose-dependent insulinotropic polypeptide ameliorates obesity-induced adipose tissue inflammation. Journal of Immunology 193(8):4002—4009.

[21] Nagashima, M., Watanabe, T., Terasaki, M., Tomoyasu, M., Nohtomi, K., Kim-Kaneyama, J., et al., 2011. Native incretins prevent the development of atherosclerotic lesions in apolipoprotein E knockout mice. Diabetologia 54(10):2649—2659.

[22] Nogi, Y., Nagashima, M., Terasaki, M., Nohtomi, K., Watanabe, T., Hirano, T., 2012. Glucose-dependent insulinotropic polypeptide prevents the progression of macrophage-driven atherosclerosis in diabetic apolipoprotein E-null mice. PLoS One 7(4):e35683.

[23] Terasaki, M., Yashima, H., Mori, Y., Saito, T., Shiraga, Y., Kawakami, R., et al., 2021. Glucose-dependent insulinotropic polypeptide suppresses foam cell formation of macrophages through inhibition of the cyclin-dependent kinase 5-CD36 pathway. Biomedicines 9(7).

[24] Miyawaki, K., Yamada, Y., Ban, N., Ihara, Y., Tsukiyama, K., Zhou, H., et al., 2002. Inhibition of gastric inhibitory polypeptide signaling prevents obesity. Nature Medicine 8(7):738—742.

[25] Goettsch, C., Hutcheson, J.D., Hagita, S., Rogers, M.A., Creager, M.D., Pham, T., et al., 2016. A single injection of gain-of-function mutant PCSK9 adeno-associated virus vector induces cardiovascular calcification in mice with no genetic modification. Atherosclerosis, 251109—251118.

[26] Bjorklund, M.M., Hollensen, A.K., Hagensen, M.K., Dagnaes-Hansen, F., Christoffersen, C., Mikkelsen, J.G., et al., 2014. Induction of atherosclerosis in mice and hamsters without germline genetic engineering. Circulation Research 114(11):1684—1689.

[27] McLean, B.A., Wong, C.K., Kaur, K.D., Seeley, R.J., Drucker, D.J., 2021. Differential importance of endothelial and hematopoietic cell GLP-1Rs for cardiometabolic versus hepatic actions of semaglutide. JCI Insight 6(22).

[28] Daugherty, A., Whitman, S.C., 2003. Quantification of atherosclerosis in mice. Methods in Molecular Biology, 209293—209309.

[29] Yusta, B., Baggio, L.L., Koehler, J., Holland, D., Cao, X., Pinnell, L.J., et al., 2015. GLP-1 receptor (GLP-1R) agonists modulate enteric immune responses through the intestinal intraepithelial lymphocyte (IEL) GLP-1R. Diabetes 64(7):2537—2549.

[30] Pujadas, G., Varin, E.M., Baggio, L.L., Mulvihill, E.E., Bang, K.W.A., Koehler, J.A., et al., 2020. The gut hormone receptor GIPR links energy availability to the control of hematopoiesis. Molecular Metabolism 39101008.

[31] Hansotia, T., Maida, A., Flock, G., Yamada, Y., Tsukiyama, K., Seino, Y., et al., 2007. Extrapancreatic incretin receptors modulate glucose homeostasis, body weight, and energy expenditure. Journal of Clinical Investigation 117(1):143—152.

[32] Mantelmacher, F.D., Fishman, S., Cohen, K., Pasmanik Chor, M., Yamada, Y., Zvibel, I., et al., 2017. Glucose-dependent insulinotropic polypeptide receptor deficiency leads to impaired bone marrow hematopoiesis. Journal of Immunology 198(8):3089—3098.

[33] Nagareddy, P.R., Murphy, A.J., Stirzaker, R.A., Hu, Y., Yu, S., Miller, R.G., et al., 2013. Hyperglycemia promotes myelopoiesis and impairs the resolution of atherosclerosis. Cell Metabolism 17(5):695—708.

[34] Getty-Kaushik, L., Song, D.H., Boylan, M.O., Corkey, B.E., Wolfe, M.M., 2006. Glucose-dependent insulinotropic polypeptide modulates adipocyte lipolysis and reesterification. Obesity 14(7):1124—1131.

[35] Joo, E., Harada, N., Yamane, S., Fukushima, T., Taura, D., Iwasaki, K., et al., 2017. Inhibition of gastric inhibitory polypeptide receptor signaling in adipose tissue reduces insulin resistance and hepatic steatosis in high-fat diet-fed mice. Diabetes 66(4):868—879.

[36] Xu, G., Kaneto, H., Laybutt, D.R., Duvivier-Kali, V.F., Trivedi, N., Suzuma, K., et al., 2007. Downregulation of GLP-1 and GIP receptor expression by hyperglycemia: possible contribution to impaired incretin effects in diabetes. Diabetes 56(6):1551—1558.

[37] Lynn, F.C., Pamir, N., Ng, E.H., McIntosh, C.H., Kieffer, T.J., Pederson, R.A., 2001. Defective glucose-dependent insulinotropic polypeptide receptor expression in diabetic fatty Zucker rats. Diabetes 50(5):1004—1011.

[38] Hojberg, P.V., Vilsboll, T., Rabol, R., Knop, F.K., Bache, M., Krarup, T., et al., 2009. Four weeks of near-normalisation of blood glucose improves the insulin response to glucagon-like peptide-1 and glucose-dependent insulinotropic polypeptide in patients with type 2 diabetes. Diabetologia 52(2):199—207.

[39] West, J.A., Tsakmaki, A., Ghosh, S.S., Parkes, D.G., Gronlund, R.V., Pedersen, P.J., et al., 2021. Chronic peptide-based GIP receptor inhibition exhibits modest glucose metabolic changes in mice when

administered either alone or combined with GLP-1 agonism. PLoS One 16(3):e0249239.

[40] Newman, A.A., Baylis, R.A., Hess, D.L., Griffith, S.D., Shankman, L.S., Cherepanova, O.A., et al., 2018. Irradiation abolishes smooth muscle investment into vascular lesions in specific vascular beds. JCI Insight 3(15).

[41] Schiller, N.K., Kubo, N., Boisvert, W.A., Curtiss, L.K., 2001. Effect of gamma-irradiation and bone marrow transplantation on atherosclerosis in LDL receptor-deficient mice. Arteriosclerosis, Thrombosis, and Vascular Biology 21(10):1674—1680.

[42] Patel, J., Douglas, G., Kerr, A.G., Hale, A.B., Channon, K.M., 2018. Effect of irradiation and bone marrow transplantation on angiotensin II-induced aortic inflammation in ApoE knockout mice. Atherosclerosis, 27674-82.

[43] Ikeda, J., Scipione, C.A., Hyduk, S.J., Althagafi, M.G., Atif, J., Dick, S.A., et al., 2021. Radiation impacts early atherosclerosis by suppressing intimal LDL accumulation. Circulation Research 128(4):530—543.

[44] Mori, Y., Kushima, H., Koshibu, M., Saito, T., Hiromura, M., Kohashi, K., et al., 2018. Glucose-dependent insulinotropic polypeptide suppresses peripheral arterial remodeling in male mice. Endocrinology 159(7):2717—2732.

[45] Bowker, N., Hansford, R., Burgess, S., Foley, C.N., Auyeung, V.P.W., Erzurumluoglu, A.M., et al., 2021. Genetically predicted glucose-dependent insulinotropic polypeptide (GIP) levels and cardiovascular disease risk are driven by distinct causal variants in the GIPR region. Diabetes 70(11):2706—2719.

[46] Jujic, A., Nilsson, P.M., Atabaki-Pasdar, N., Dieden, A., Tuomi, T., Franks, P.W., et al., 2021. Glucose-dependent insulinotropic peptide in the high-normal range is associated with increased carotid intima-media thickness. Diabetes Care 44(1):224—230.

[47] Gogebakan, O., Osterhoff, M.A., Schuler, R., Pivovarova, O., Kruse, M., Seltmann, A.C., et al., 2015. GIP increases adipose tissue expression and blood levels of MCP-1 in humans and links high energy diets to inflammation: a randomised trial. Diabetologia 58(8):1759—1768.

[48] Kizilkaya, H.S., Sorensen, K.V., Kibsgaard, C.J., Gasbjerg, L.S., Hauser, A.S., Sparre-Ulrich, A.H., et al., 2021. Loss of function glucose-dependent insulinotropic polypeptide receptor variants are associated with alterations in BMI, bone strength and cardiovascular outcomes. Frontiers in Cell and Developmental Biology 9749607.

[49] Karhunen, V., Daghlas, I., Zuber, V., Vujkovic, M., Olsen, A.K., Knudsen, L.B., et al., 2021. Leveraging human genetic data to investigate the cardiometabolic effects of glucose-dependent insulinotropic polypeptide signalling. Diabetologia 64(12):2773—2778.

[50] Baggio, L.L., Drucker, D.J., 2021. Glucagon-like peptide-1 receptor co-agonists for treating metabolic disease. Molecular Metabolism 46101090.

[51] Wilson, J.M., Lin, Y., Luo, M.J., Considine, G., Cox, A.L., Bowsman, L.M., et al., 2022. The dual glucose-dependent insulinotropic polypeptide and glucagon-like peptide-1 receptor agonist tirzepatide improves cardiovascular risk biomarkers in patients with type 2 diabetes: a post hoc analysis. Diabetes, Obesity and Metabolism 24(1):148—153.

[52] Sattar, N., McGuire, D.K., Pavo, I., Weerakkody, G.J., Nishiyama, H., Wiese, R.J., et al., 2022. Tirzepatide cardiovascular event risk assessment: a pre-specified meta-analysis. Nature Medicine 28(3):591—598.

[53] Kahles, F., Liberman, A., Halim, C., Rau, M., Mollmann, J., Mertens, R.W., et al., 2018. The incretin hormone GIP is upregulated in patients with atherosclerosis and stabilizes plaques in ApoE(-/-) mice by blocking monocyte/macrophage activation. Molecular Metabolism, 14150—14157.

Supplementary Figure 1

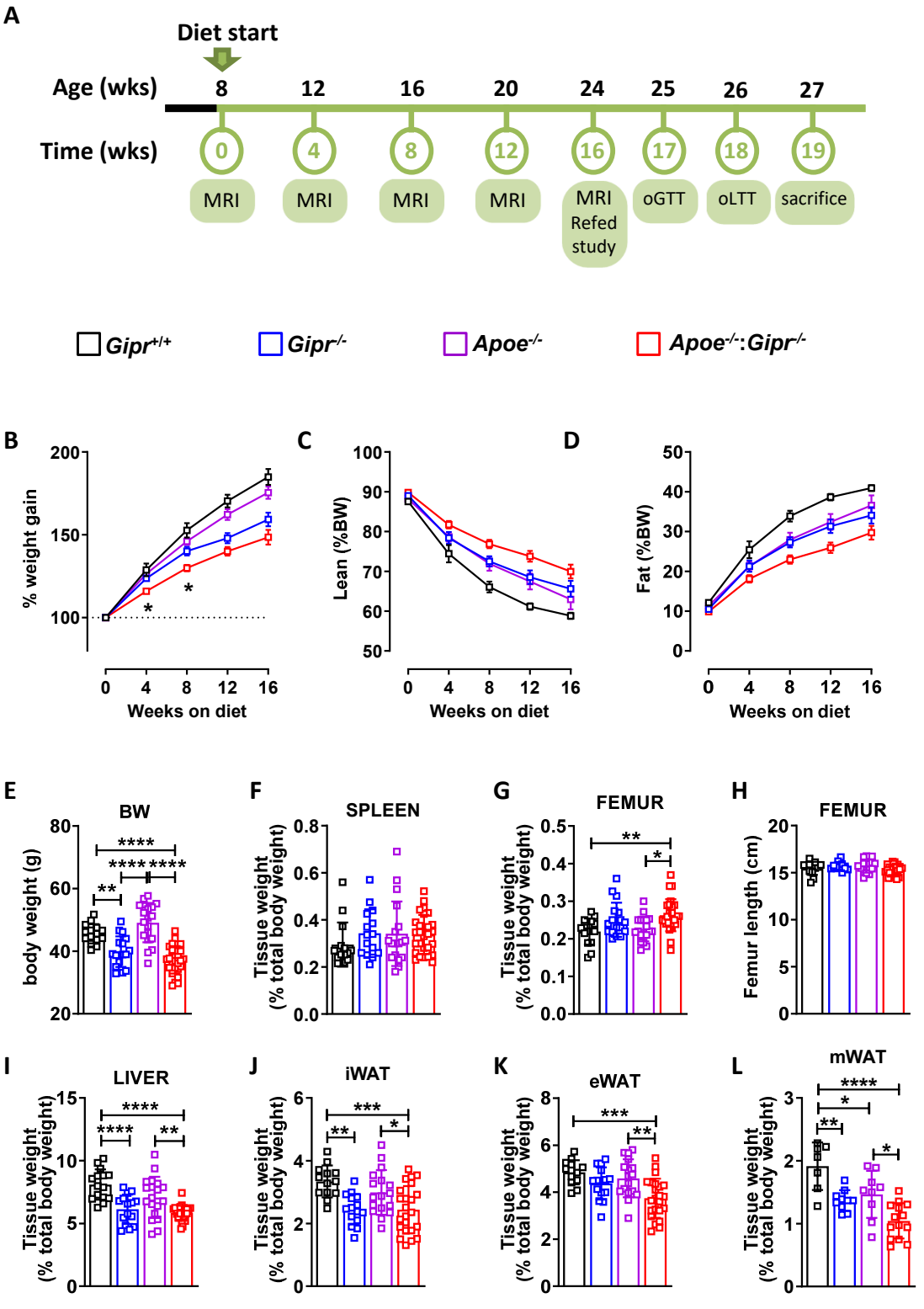

Supplementary Figure 2

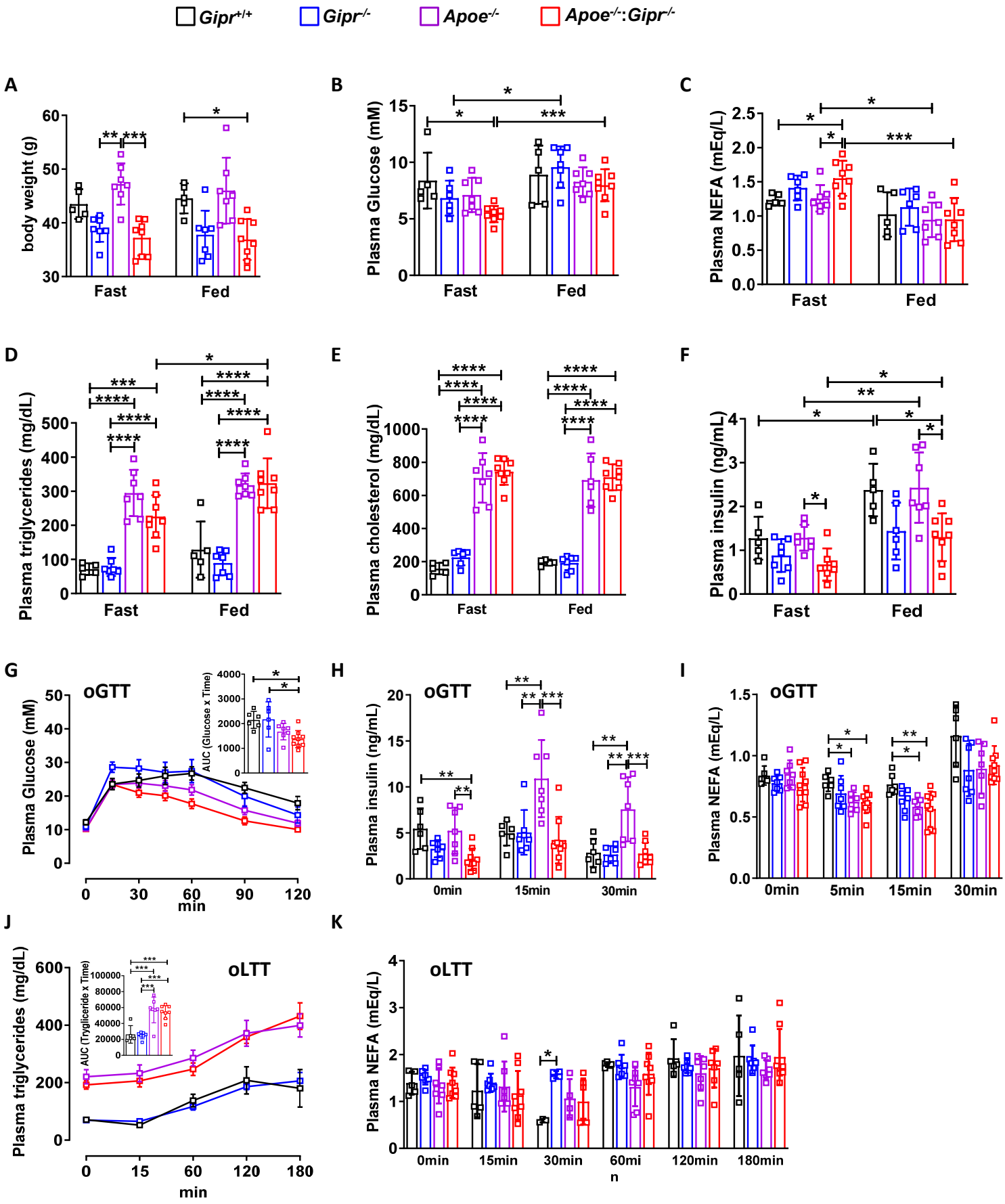

Supplementary Figure 3

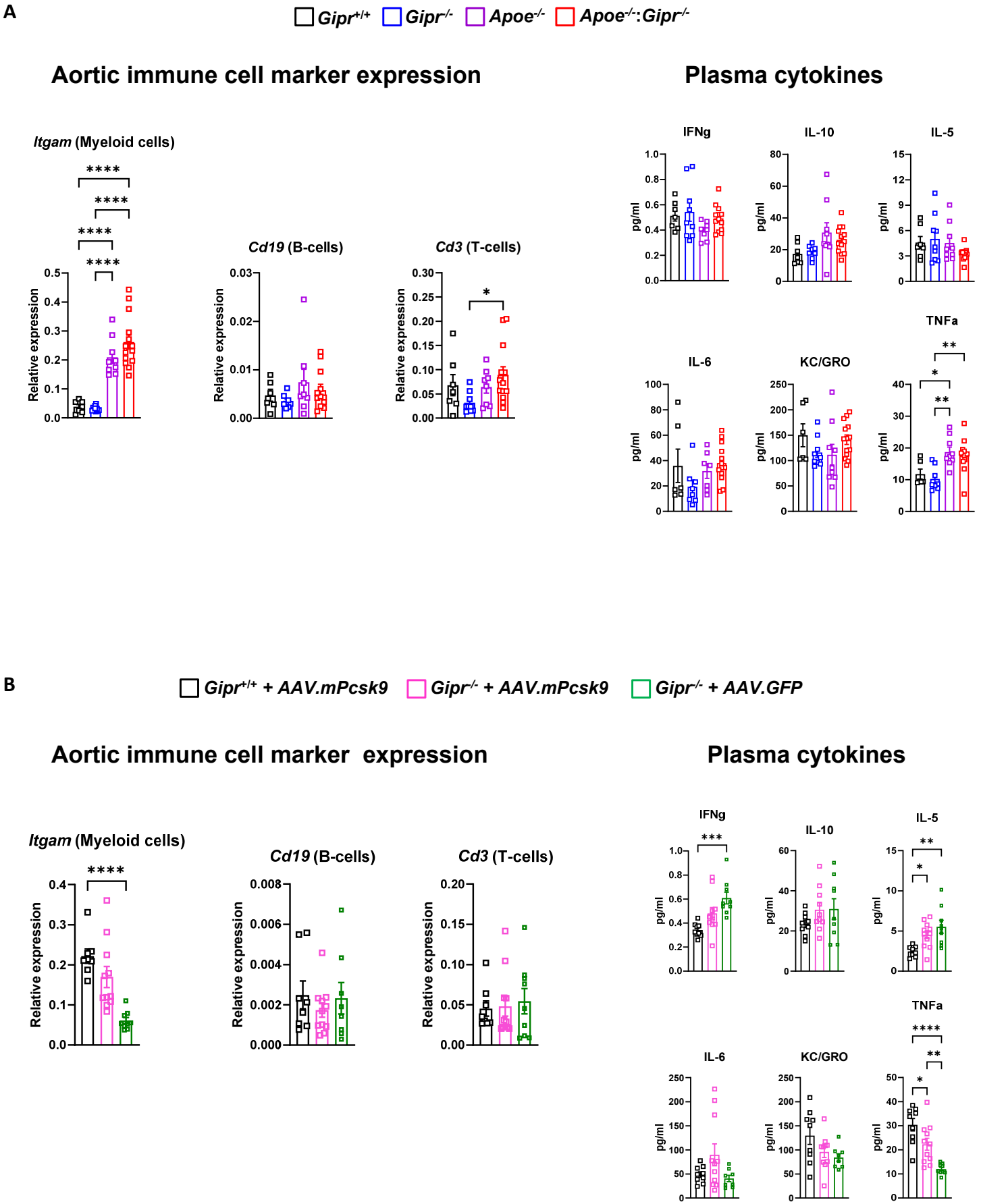

Supplementary Figure 4

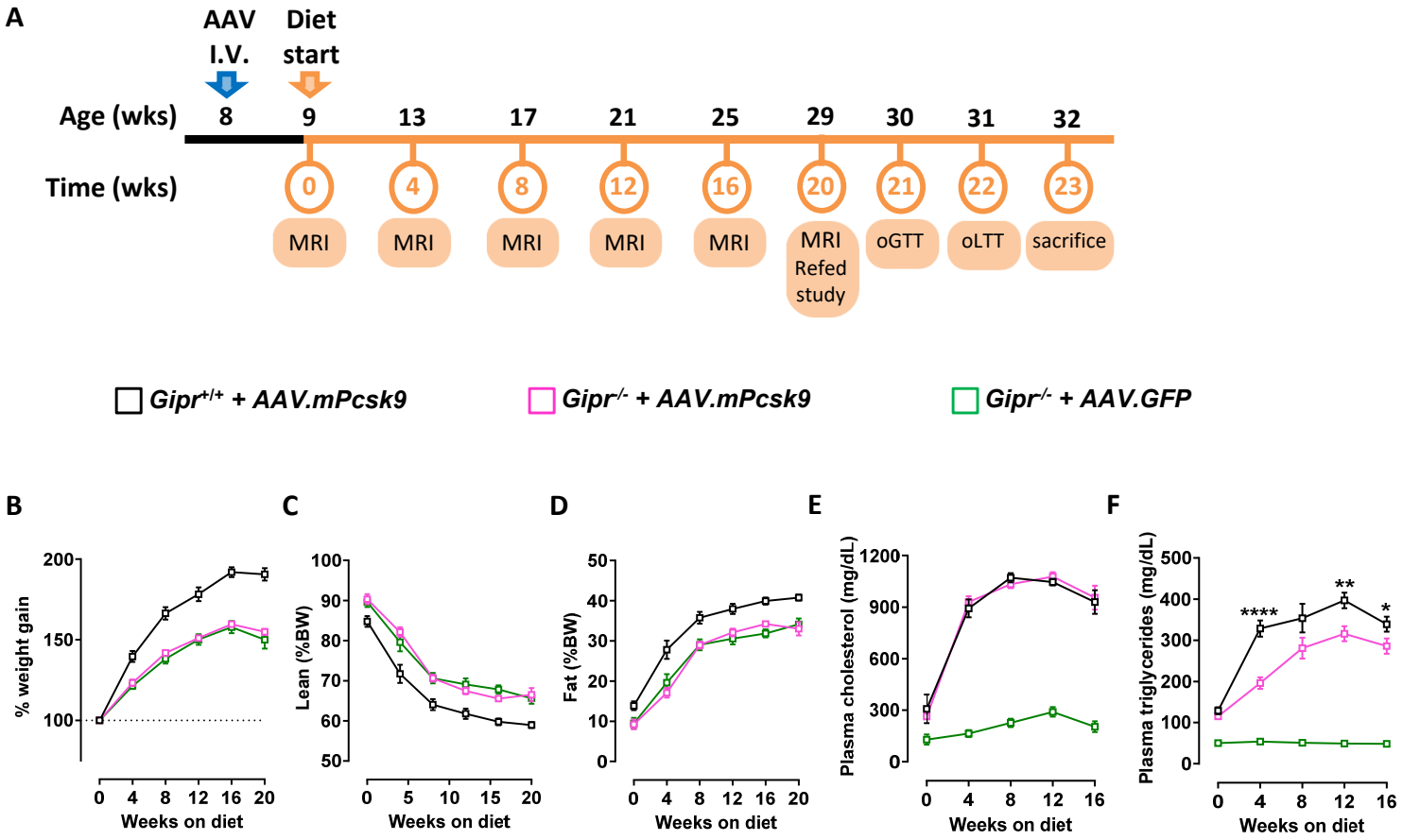

Supplementary Figure 5

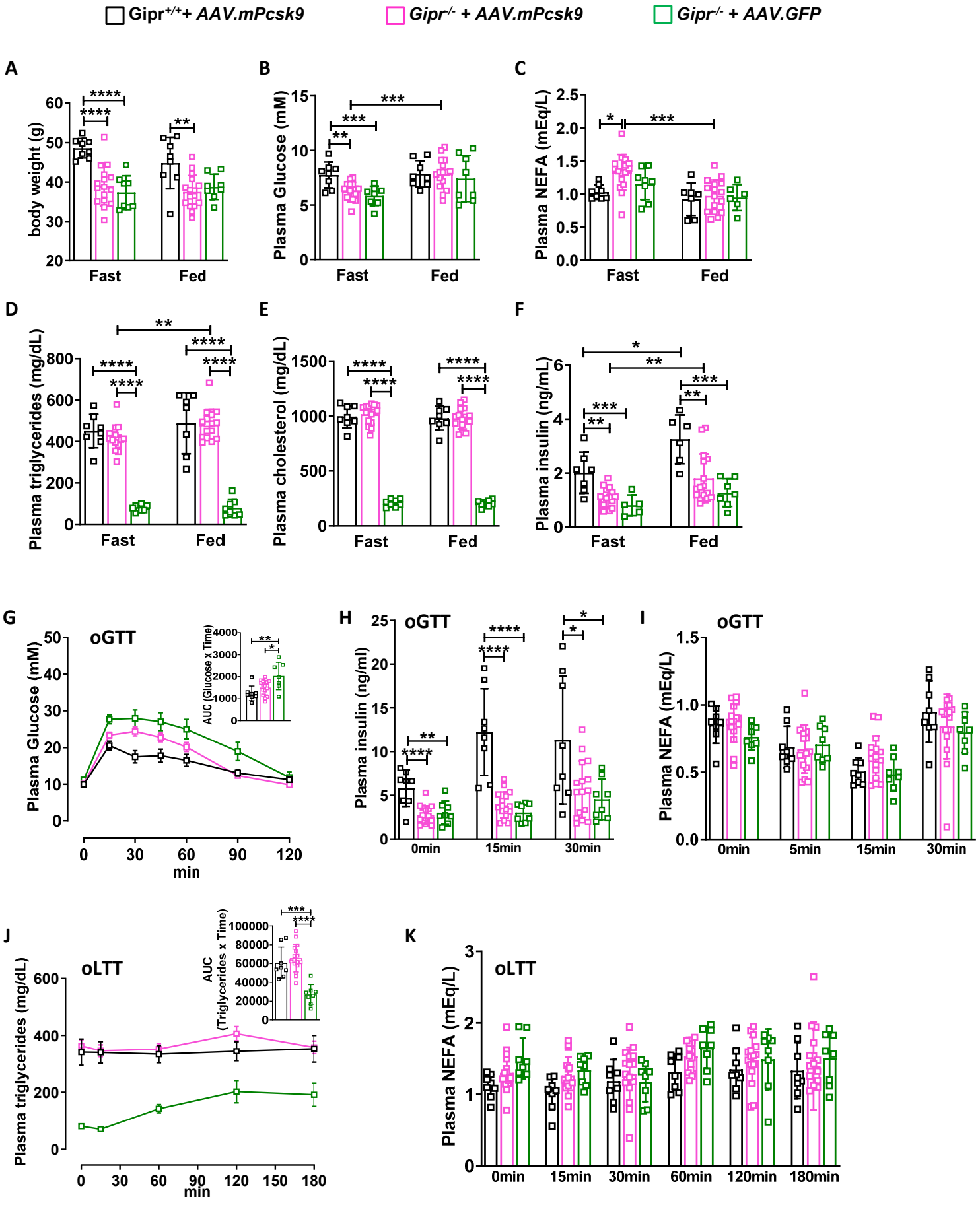

Supplementary Figure 6

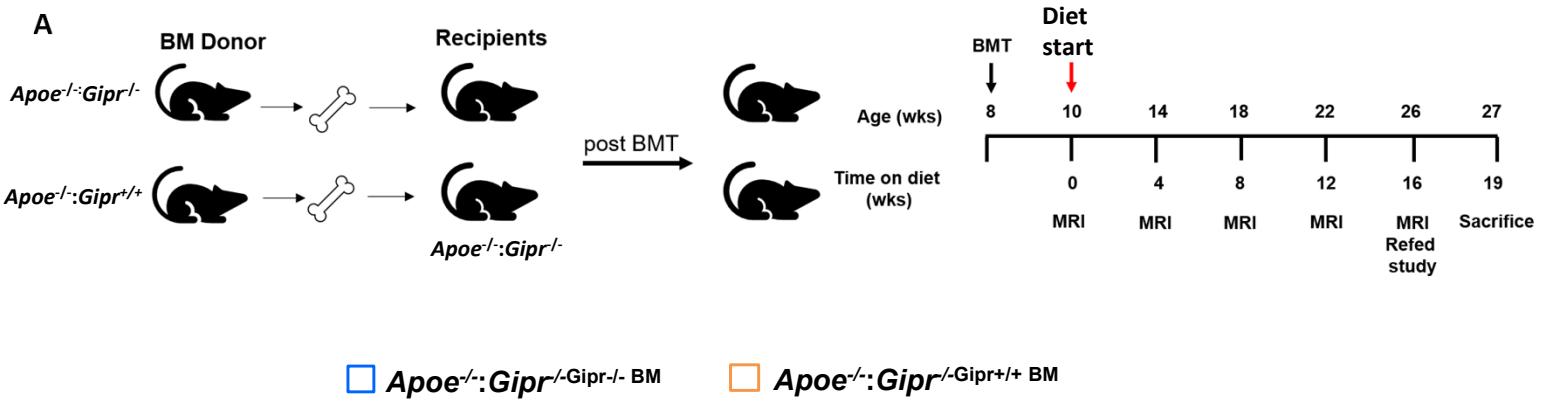

Apoe-/-:Gipr-/-Gipr-/- BM Apoe-/-:Gipr-/-Gipr+/+ BM

B Peripheral blood

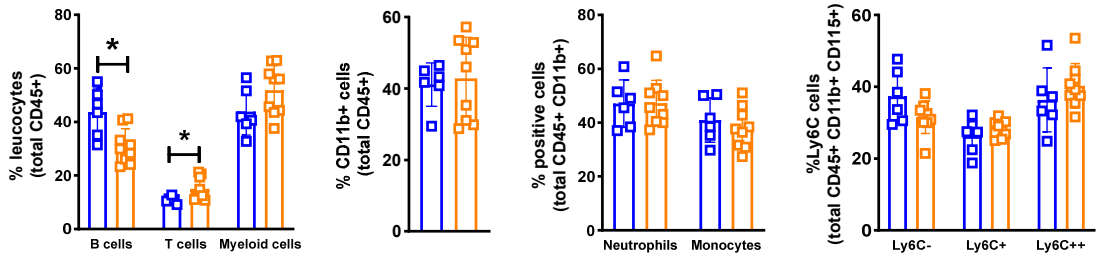

C Aorta gene expression

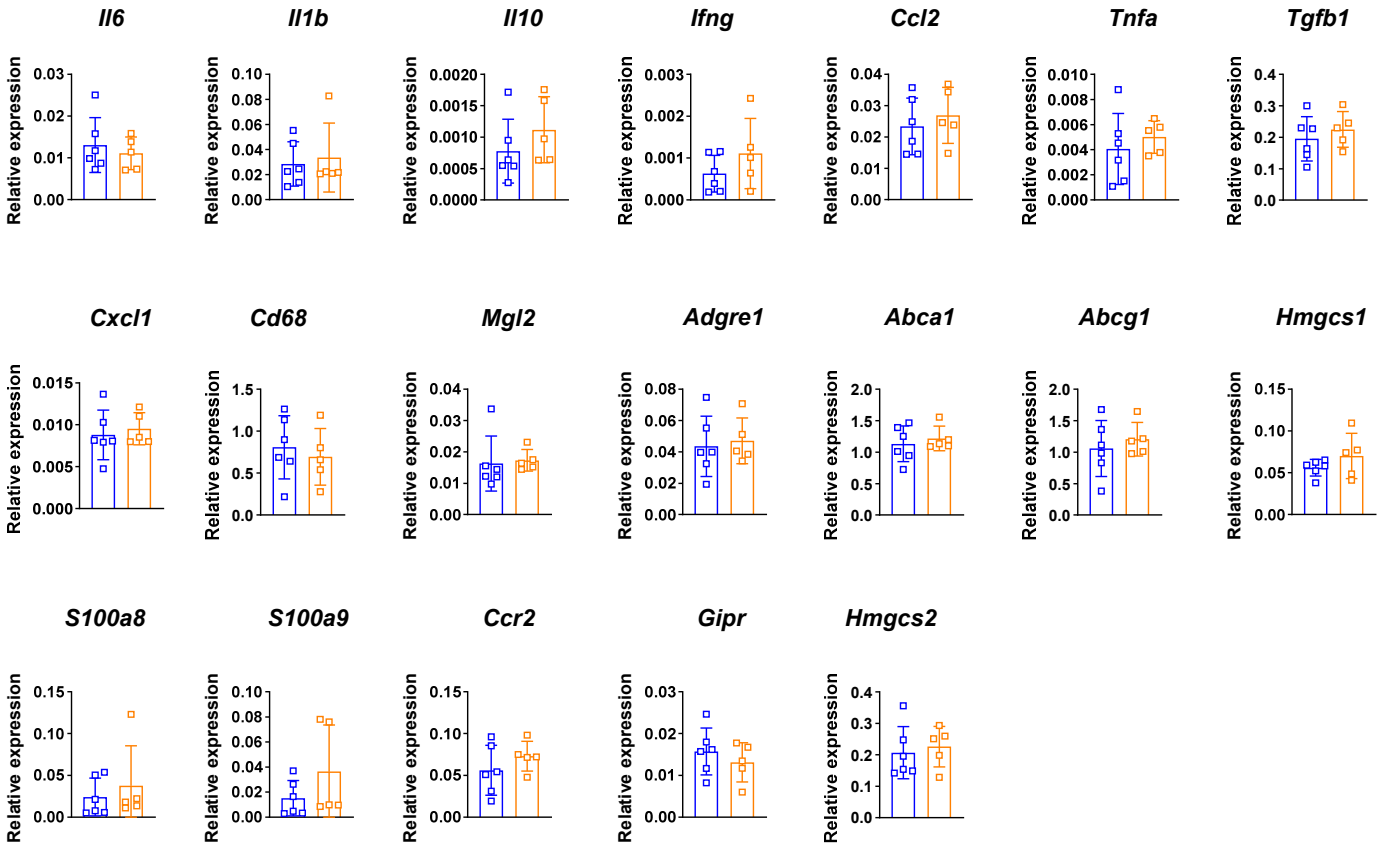

Supplementary Figure 7

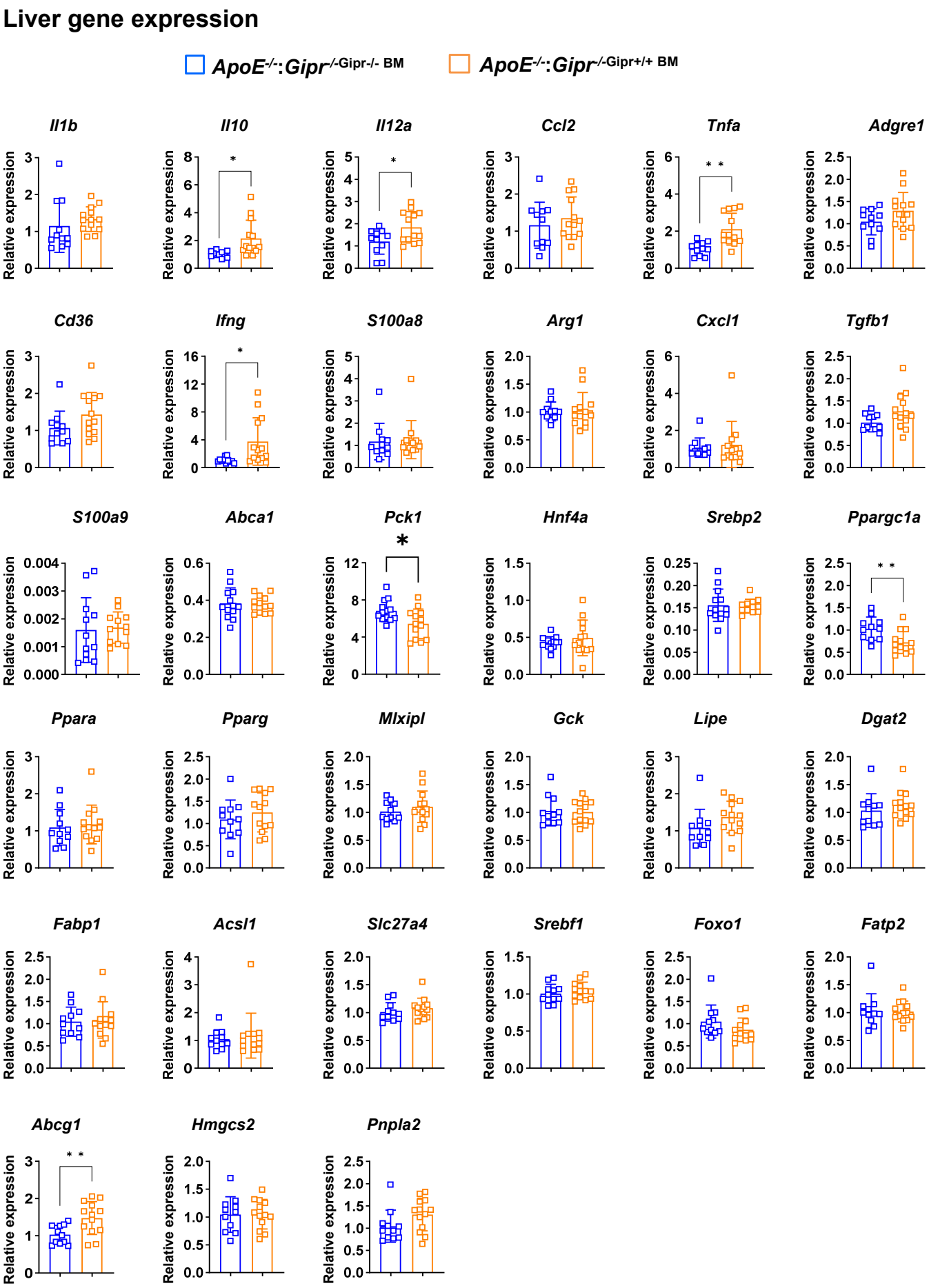

Supplementary Figure Legends

Supplementary Figure 1. Body composition and tissue weights in proatherogenic diet-fed *ApoE*$^{-/-}$:*Gipr*$^{-/-}$ and control mice. (A) Schematic depiction of the timeline for studies in *ApoE*$^{-/-}$:*Gipr*$^{-/-}$ and control mice. Starting at 8 weeks of age, all mice were fed a proatherogenic diet for a total of 19 weeks. Magnetic resonance imaging (MRI) was performed at baseline and at 4, 8, 12 and 16 weeks after diet commencement. Fasting-refeeding studies, oral glucose tolerance (oGTT), and oral lipid tolerance (oLTT) tests were performed after 16, 17 and 18 weeks, and mice were sacrificed after 19 weeks of proatherogenic diet feeding, respectively. Change in body weight (B) and body composition (C, D) during the first 16 weeks of proatherogenic diet feeding. Body weight (E), indicated tissue weights normalized to body weight (F, G, I-L), and femur length (H) in mice after 19 weeks of maintenance on the proatherogenic diet. Data are mean ± SEM (panels B-D) or ± SD (panels E-L). n=9 – 27 mice per group. * $P \leq 0.05$, ** $P \leq 0.01$, *** $P \leq 0.001$, **** $P \leq 0.0001$.

Supplementary Figure 2. Metabolic measurements during fasting-refeeding studies and glucose and lipid tolerance tests in *ApoE*$^{-/-}$:*Gipr*$^{-/-}$ and control mice fed a proatherogenic diet. (A) body weight, and plasma levels of glucose (B), non-esterified fatty acids (NEFA, C), triglycerides (D), cholesterol (E), and insulin (F) in *ApoE*$^{-/-}$:*Gipr*$^{-/-}$ and control mice during fasting and refeeding studies performed after 16 weeks of proatherogenic diet feeding. Plasma glucose (G), insulin (H) and NEFA (I) levels during an oral glucose tolerance test (oGTT), and plasma triglycerides (J) and NEFA (K) levels during an oral lipid tolerance test (oLTT) in *ApoE*$^{-/-}$:*Gipr*$^{-/-}$ and control mice after 17 and 18 weeks of proatherogenic diet feeding, respectively. Data are mean ± SD (panels A-F, H, I and K) or ± SEM (panels G and J). n=5 – 9 mice per group. * $P \leq 0.05$, ** $P \leq 0.01$, *** $P \leq 0.001$, **** $P \leq 0.0001$.

Supplementary Figure 3. Aortic gene expression of cell-type-specific markers and plasma cytokine levels in experimental mice. Aortic mRNA and plasma cytokine levels in proatherogenic diet-fed (A) *Apoe*$^{-/-}$:*Gipr*$^{-/-}$ and control mice, and (B) PCSK9-treated *Gipr*$^{-/-}$ and control mice. Data are mean ± SEM. n=6 – 14 mice per group. * $P \leq 0.05$, ** $P \leq 0.01$, ***$P \leq 0.001$, **** $P \leq 0.0001$.

Supplementary Figure 4. Body composition, plasma lipids and tissue weights in AAV-PCSK9-treated *Gipr-/-* mice vs. AAV-PCSK-9-treated *Gipr+/+* and AAV-GFP-treated *Gipr-/-* control mice fed a proatherogenic diet. (A) Schematic depiction of the timeline for studies done in AAV-PCSK9-treated *Gipr-/-* and control mice. Regular chow fed mice were treated with PCSK9 (AAV.mPcsk9) or control (AAV-GFP) adeno-associated virus at 8 weeks of age and then the following week were switched to a proatherogenic diet for 23 weeks. Magnetic resonance imaging (MRI) was performed at baseline and at 4, 8, 12, 16 and 20 weeks after diet commencement. Fasting-refeeding studies, oral glucose tolerance (oGTT), and oral lipid tolerance (oLTT) tests were performed after 20, 21 and 22 weeks, and mice were sacrificed after 23 weeks of proatherogenic

diet feeding, respectively. Change in body weight (B) and body composition (C, D) during the first 20 weeks of proatherogenic diet feeding. Plasma cholesterol (E), and triglyceride (F) levels during the first 16 weeks of proatherogenic diet. Tissue weights normalized to body weight (G-I, K-N), and femur length (J) in mice after 23 weeks of maintenance on the proatherogenic diet. Data are mean ± SEM (panels B-F) or ± SD (panels G-N). n=8 – 29 mice per group. * $P \leq 0.05$, ** $P \leq 0.01$, **** $P \leq 0.0001$.

Supplementary Figure 5. Metabolic measurements during fasting-refeeding studies and glucose and lipid tolerance tests in proatherogenic diet-fed AAV-PCSK9-treated *Gipr-/-* and control mice. Body weight (A), and plasma levels of glucose (B), non-esterified fatty acids (NEFA, C), triglycerides (D), cholesterol (E), and insulin (F) in AAV-PCSK9-treated *Gipr-/-* and control mice during fasting and refeeding studies performed after 20 weeks of proatherogenic diet feeding. Plasma glucose (G), insulin (H), and NEFA (I) levels during an oral glucose tolerance test (oGTT), and plasma triglycerides (J) and NEFA (K) levels during an oral lipid tolerance test (oLTT) in AAV-PCSK9-treated *Gipr-/-* and control mice after 21 and 22 weeks of proatherogenic diet feeding, respectively. Data are mean ± SD (panels A-F, H, I and K) or ± SEM (panels G and J). n=5 – 16 mice per group. * $P \leq 0.05$, ** $P \leq 0.01$, *** $P \leq 0.001$, **** $P \leq 0.0001$.

Supplementary Figure 6. Peripheral blood immune cell populations and aortic gene expression in mice following bone marrow-specific restoration of Gipr expression in mice fed a proatherogenic diet. (A) Schematic depiction of the timeline for the experiments. At 8 weeks of age, regular chow fed *ApoE*$^{-/-}$:*Gipr*$^{-/-}$ mice received a bone marrow transplant from *ApoE*$^{-/-}$:*Gipr*$^{-/-}$ (*ApoE*$^{-/-}$:*Gipr*$^{-/-\text{Gipr-/-BM}}$) or *ApoE*$^{-/-}$:*Gipr*$^{+/+}$ (*ApoE*$^{-/-}$:*Gipr*$^{-/-\text{Gipr+/+BM}}$) mice. Two weeks later, mice were switched to a proatherogenic diet. Magnetic resonance imaging (MRI) was performed at baseline and at 4, 8, 12 and 16 weeks after diet commencement. Fasting-refeeding studies were performed after 16 weeks, and mice were sacrificed after 19 weeks of proatherogenic diet feeding. (B) Proportions of circulating immune cells. (C) Aortic mRNA expression levels of genes associated with inflammation. Data are mean ± SD. n=5 - 9 mice per group. * $P \leq 0.05$.

Supplementary Figure 7. Hepatic gene expression in mice following bone marrow-specific restoration of Gipr expression in mice fed a proatherogenic diet for 19 weeks. Liver mRNA expression levels of genes associated with inflammation and glucose and lipid metabolism. Data are mean ± SD. n=11 - 13 mice per group. * $P \leq 0.05$, ** $P \leq 0.01$.